HHS Public Access

Author manuscript

Cell. Author manuscript; available in PMC 2024 September 14.

Published in final edited form as:

Cell. 2023 September 14; 186(19): 4172–4188.e18. doi:10.1016/j.cell.2023.08.008.

PINK1, Keap1 and Rtnl1 regulate selective clearance of endoplasmic reticulum during development

Ruoxi Wang[1], **Tina M. Fortier**[1], **Fei Chai**[1], **Guangyan Miao**[1], **James L. Shen**[1], **Lucas J. Restrepo**[1], **Jeromy J. DiGiacomo**[1], **Panagiotis D. Velentzas**[1], **Eric H. Baehrecke**[1,2,*]

[1]Department of Molecular, Cell and Cancer Biology, University of Massachusetts Chan Medical School, Worcester, MA 01605 USA

[2]Lead contact

SUMMARY

Selective clearance of organelles, including endoplasmic reticulum (ER) and mitochondria, by autophagy plays an important role in cell health. Here we describe a developmentally programmed selective ER clearance by autophagy. We show that Parkinson's disease associated PINK1, as well as Atl, Rtnl1 and Trp1 receptors, regulate ER clearance by autophagy. The E3 ubiquitin ligase Parkin functions downstream of PINK1 and is required for mitochondrial clearance while having the opposite function in ER clearance. By contrast, Keap1 and the E3 ubiquitin ligase Cullin3 function downstream of PINK1 to regulate ER clearance by influencing Rtnl1 and Atl. PINK1 regulates a change in Keap1 localization and Keap1-dependent ubiquitylation of the ER-phagy receptor Rtnl1 to facilitate ER clearance. Thus, PINK1 regulates the selective clearance of ER and mitochondria by influencing the balance of Keap1- and Parkin-dependent ubiquitylation of substrates that determine which organelle is removed by autophagy.

Graphical Abstract

*Correspondence to Eric H. Baehrecke, Department of Molecular, Cell and Cancer Biology, 423 Lazare Research Building, 364 Plantation St., University of Massachusetts Chan Medical School, Worcester, MA 01605, USA. Telephone: +1-508-856-6733, eric.baehrecke@umassmed.edu.

AUTHOR CONTRIBUTIONS: R.W. and E.H.B. designed experiments, R.W., T.M.F., F.C., G.M., J.L.S., L.J.R., J.J.D., and P.D.V. performed experiments. R.W., P.D.V. and E.H.B. wrote the manuscript and all authors commented on it.

DECLARATION OF INTERESTS:

The authors declare no competing interests.

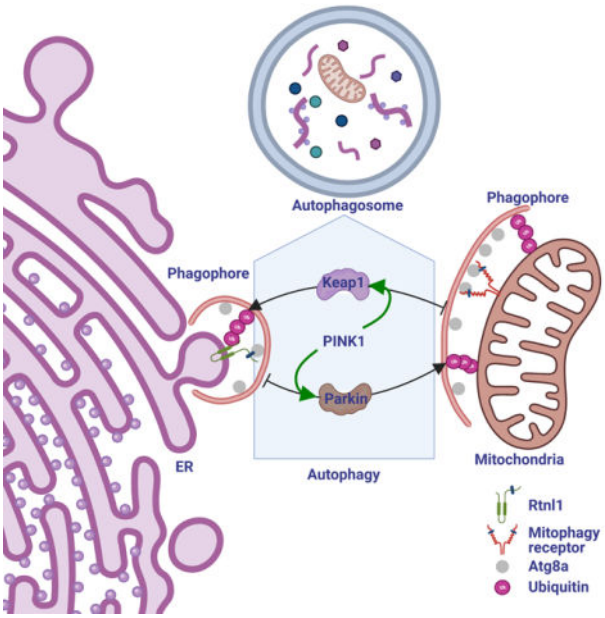

In Brief

Investigation into the clearance of endoplasmic reticulum (ER) during fly intestine development unveils a crosstalk between mitophagy and ER-phagy, and provides mechanistic insights into autophagy-mediated cross-organelle remodeling that is important for cell- and organism- health.

INTRODUCTION

Macroautophagy (autophagy) is a catabolic process that facilitates the degradation of either bulk non-specific cytoplasmic components or specific cytoplasmic cargoes, including mitochondria and ER, by delivery to lysosomes. The selective removal of each type of organelle by autophagy depends on specific initiation signals and receptors[1,2]. For example, the clearance of mitochondria by autophagy (mitophagy) is triggered when stimuli induce stabilization of the PTEN-induced kinase 1 (PINK1) on the surface of mitochondria[3]. PINK1 then phosphorylates ubiquitin and the E3 ubiquitin ligase Parkin on mitochondria[4,5], thus marking mitochondria and associated proteins with ubiquitin to target them for degradation by autophagy[6–9].

The recruitment of mitochondria into forming autophagosomes depends on receptors that bind to both ubiquitin and the core autophagy protein LC3/GABARAP (Atg8 in lower organisms)[10,11]. Similarly, selective clearance of ER by autophagy (ER-phagy) requires receptors for recruitment of ER into forming autophagosomes[12–19]. Importantly, the signal and receptor codes that mediate and distinguish selective mitophagy from ER-phagy are thought to be unique for mitochondria and ER.

The mechanisms that distinguish mitophagy and ER-phagy within a single cell has been challenging. This is because of limitations in the availability of physiological models to study the clearance of specific organelles within a single cell. In addition, the mechanisms

that control organelle-specific autophagy is largely based on the use of chemicals that stress either mitochondria or ER in cultured cells. It remains unclear if different autophagy cargoes are cleared by distinct programs within the same cell, and how organelle-specific genetic regulatory programs influence one another.

Here we show that mitochondria and ER are differentially cleared by autophagy in a single cell during development in the *Drosophila* intestine. Although mitochondria and ER require common autophagy genes for clearance, each organelle utilizes specific receptors for removal. Mitochondrial PINK1 is required for ER-phagy even though it is thought to specifically influence mitophagy. The E3 ubiquitin ligase Parkin that functions downstream of PINK1 in mitophagy has the opposite function in ER-phagy. By contrast, the Keap1 and Cullin3 E3 ubiquitin ligase complex is required for ER-phagy downstream of PINK1. PINK1 influences the localization of Keap1, and PINK1 and Keap1 are required for ubiquitylation of the ER-phagy receptor Rtnl1. Our data indicates that PINK1 regulates the clearance of ER and mitochondria, and organelle-specificity is achieved through the functions of either Keap1 or Parkin.

RESULTS

ER clearance is regulated by autophagy during development

A rise in steroid triggers the development from a larva to prepupa in *Drosophila*, and induces autophagy in enterocyte cells of the intestine anterior midgut[20]. This autophagy is specific to enterocytes, and is required for cell size reduction. Mitochondria are removed in an autophagy (*Atg*) gene-dependent manner from enterocytes[20,21]. However, it is unclear if ER is cleared by autophagy from enterocytes. Transmission electron microscopy (TEM) analyses of control enterocytes 2 hours after puparium formation (APF) revealed autophagosomes that contain rough ER (Figure 1A). By contrast, $Atg8a^{\Delta}$ mutant intestine enterocytes exhibit decreased autophagosome structures and possess numerous dilated ER structures (Figure 1B and 1C, Figure S1A–S1B). The presence of dilated ER in *Atg8a* mutant cells is consistent with the ER morphology observed in ER-phagy receptor deficient mammalian cells[12].

To investigate whether ER degradation requires autophagy in *Drosophila* intestine cells, we examined ER-localized Sec61α-GFP reporter clearance in autophagy mutant enterocytes 2 hours APF. Cells lacking the function of either *Atg9, Atg16,* or *Vps34* exhibit increased levels of Sec61α-GFP compared to neighboring control cells (Figure 1D–1G, Figure S1C–S1D). Consistent with loss of autophagy, $Atg9^{d51}$, $Atg16^{\Delta}$ and $Vps34^{m22}$mutant intestine cells possessed increased levels of the autophagy receptor and substrate Ref(2)p (p62 in mammals), and elevated levels of the ER-localized Calnexin protein compared to neighboring control cells (Figure S1E–S1J). Similarly, Calnexin protein levels increased in *Atg1* and *Atg9* knockdown intestines compared to control intestines expressing Luciferase RNAi (Figure 1H and 1I). Additionally, homozygous $Atg16^{\Delta}$ mutant intestines possess 55% more Calnexin protein compared to control w^{1118} intestines (Figure 1J and 1K).

We constructed an ER-phagy sensor to investigate the dynamics of ER autophagic flux. Tandem fluorochromes, including modified pH sensitive pHluorin and pH resistant mKate2,

were fused in between the ER-targeting sequence of Bip and a KDEL-ER retention signal, and placed under control of a UAS promoter (UAS-ss-pHluorin-mKate2-KDEL-V5, Figure 1L) to measure ER-phagy in the intestine. Both green and red fluorochromes of the sensor exhibit ER-like structures in third instar larval intestine cells before the initiation of autophagy (Figure S1K)[20]. Additionally, ss-pHluorin-mKate2-KDEL-V5 levels in *Atg16*$^{\Delta}$ mutant larval intestines are similar to control intestines (Figure S1L–S1M). After activation of autophagy, the ss-pHluorin-mKate2-KDEL-containing ER fragments are delivered to autophagosomes followed by fusion with lysosomes, causing a lack of green fluorescence due to the acidic nature of autolysosomes (Figure 1M). Consistent with the requirement for autophagy in ER clearance, ss-pHluorin-mKate2-KDEL-V5 reporter levels are elevated in *Atg16*$^{\Delta}$ mutant enterocytes compared to control intestine cells 2 hours APF (Figure S1L–S1M). Importantly, the smaller control intestine enterocytes (Figure 1N, yellow rectangles in lower magnification images and upper panels in insets) exhibit increased ss-mKate2-KDEL puncta co-localization with lysotracker-stained lysosomes and contain less ss-pHluorin-KDEL (Figure 1N and 1O). By contrast, either *Atg9*^{d51} or *Atg16*$^{\Delta}$ mutant enterocytes are larger in size, contain more ss-pHluorin-KDEL and possess decreased ss-mKate2-KDEL puncta co-localization with lysotracker compared to control cells 2 hours APF (Figure 1N and 1O, Figure S1N–S1O).

Selective clearance of organelles requires both common genes and distinct receptors

To investigate whether ER clearance in the *Drosophila* intestine is selective, we queried the *Drosophila melanogaster* genome for ER-phagy receptors using an orthologue prediction tool[22]. Orthologues of the mammalian ER-phagy receptors ATL3, RTN3 and Sec62 are conserved and encoded by *Atl*, *Rtnl1* and *Trp1* (Figure S2A). By contrast, ER-phagy receptors FAM134B, CCPG1, TEX264 and CALCOCO1 do not possess clear fly orthologues. Significantly, *Atl*^{2}, *Rtnl1*^{1W} and *Trp1*^{KG} mutant intestine cells possess increased Sec61α-GFP ER reporter levels compared to control cells (Figure 2A–2F). In addition, Atl, Rtnl1 and Trp1 proteins interact with Atg8a *in vitro* (Figure 2G). Consistent with roles as ER-phagy receptors, Atl and Trp1 interact with Atg8a through putative LC3-interacting region (LIR) motifs (Figure S2B–S2G).

We investigated whether Rtnl1 and Atl proteins are influenced by autophagy. Antibodies do not exist against *Drosophila* ER-phagy receptors. Thus, we used CRISPR-Cas9 to tag the C-termini of both Rtnl1 and Atl with 3×Flag-V5 (Figure S2H–S2I) to enable detection of all isoforms of these ER-phagy receptors. Loss of either *Atg8a* or *Atg16* resulted in failure to clear Rtnl1 compared to control enterocytes 2 hours APF (Figure 2H–2K). Similarly, enterocyte cell loss of either *Atg9* or *Atg8a* resulted in failure to clear Atl compared to control cells 2 hours APF (Figure 2L–2O). Interestingly, loss of *Atl* mutant intestine cells exhibit an increase in Rtnl1 and Calnexin (Figure S2J–S2K). Furthermore, TEM analyses of either *Atl*^{2} or *Rtnl1*^{1W} mutant intestine enterocytes revealed increased amounts of interconnected and elongated rough ER structures in the cytoplasm that are similar to the influence of RTN3 on ER morphology in mammals[15], while control cells possessed rough ER in autophagic structures (Figure 2P–2S).

The selective recruitment of autophagic cargoes is thought to be defined by specific receptor combinations[1,2], but no studies have tested this model in a single cell in an animal. Since both mitochondria and ER clearance occur in the same intestine cell context during developmental autophagy[20,21] (Figure 1), we compared the specificities of autophagy receptors in selective mitophagy and ER-phagy. Vps13D has characteristics of an autophagy receptor[23], is required for clearance of mitochondria[21,23], influences mitochondria ER contact[24], and ER morphology[25]. Consistent with previous work[21,23], *Vps13D*^{MI} mutant intestine cells exhibit increased mitochondrial Mito-GFP puncta compared to control enterocytes (Figure 3A, 3A", and 3B). Significantly, the ER protein Calnexin is elevated in the same *Vps13D*^{MI} loss-of-function intestine cells compared to neighboring control cells (Figure 3A', 3A", and 3C), thus *Vps13D* is required for both mitophagy and ER-phagy in the same cell. *Vps13D* knockdown cells also exhibit increased Sec61α-GFP compared to control cells (Figure S3A–S3B). In addition, TEM analyses of *Vps13D* mutant intestine cells accumulate dilated ER compared to control enterocytes (Figure S3C–S3D). These data indicate that ER-phagy and mitophagy share common regulators.

We investigated the functions of the Rtnl1, Trp1 and Atl ER-phagy receptors in selective ER-phagy and mitophagy. Core autophagy *Atg16*-deficient intestine enterocytes fail to clear mitochondrial-localized Mito-GFP puncta (Figure 3D and 3H), similar to how *Atg16* loss prevents ER clearance (Figure 1). By contrast, loss of either *Rtnl1*^{1W}, *Trp1*^{KG} or *Atl*^{2} in mutant intestine enterocytes fails to impact Mito-GFP puncta clearance and have similar levels to their respective neighboring control cells (Figure 3E–3H). Therefore, core regulators of autophagy impact both mitochondria and ER clearance, while the Rtnl1, Trp1 and Atl receptors are specific to ER-phagy.

We next examined if the mammalian mitophagy receptor BNIP3[26] is conserved in *Drosophila* and functions to specifically regulate the clearance of mitochondria. BNIP3 is conserved in *Drosophila*, including two amino acids in the LIR motif that are required for BNIP3 to function as a mitophagy receptor (Figure S3E–S3F). Consistent with the function of BNIP3 in mammals[26–28], fly *BNIP3* gRNAs/Cas9-expressing enterocytes possess increased mitochondrial ATP5A compared to control enterocytes (Figure 3I, 3I", and 3J). In contrast to the impact of *BNIP3* on mitochondrial clearance, ER Sec61α-GFP levels are decreased in *BNIP3* mutant compared to control intestine cells (Figure 3I'–3I" and 3K). In addition, ER-phagy flux is increased in *BNIP3* mutant enterocytes compared to control intestine cells (Figure S3H–S3J). These results indicate that BNIP3 is required for mitophagy in the same cells where Rtnl1, Trp1 and Atl are specifically required for ER-phagy.

Developmentally programmed ER clearance requires PINK1

PINK1 appears to function upstream of Vps13D in the regulation of mitophagy in intestine enterocytes[21]. Since Vps13D influences the clearance of both mitochondria and ER, we tested the influence of PINK1 on ER-phagy. Surprisingly, *PINK1*^{B9} mutant intestine enterocytes exhibit increased Sec61α-GFP and Calnexin compared to neighboring control cells (Figure 4A and 4D, Figure S4A–S4B). Similarly, *PINK1* knockdown intestine cells expressing *PINK1* RNAis exhibit elevated Sec61α-GFP compared to control cells (Figure

S4C–S4F). In addition, *Atg8a*$^{\Delta}$ loss-off-unction mutant intestine cells exhibit increased Sec61α-GFP compared to neighboring control enterocytes, and *Atg8a*$^{\Delta}$ *PINK1*^{B9} double-mutant cells exhibit similar Sec61α-GFP levels as *PINK1*^{B9} and *Atg8a*$^{\Delta}$ single-mutant intestine cells (Figure 4B–4D), indicating that *PINK1* and *Atg8a* function in the same ER-phagy pathway. Consistent with a role in ER-phagy, *PINK1*^{B9} and *PINK1*^{5} mutant intestine cells that express the ss-pHluorin-mKate2-KDEL-V5 ER-phagy sensor exhibit decreased ss-mKate2-KDEL puncta co-localization with lysotracker compared to control intestines (Figure S4G–S4J).

PINK1 is localized to and activated on mitochondria to regulate phosphorylation of ubiquitin (serine 65) and ubiquitination of multiple mitochondria-associated proteins[7,9,10]. Since PINK1 regulates clearance of both mitochondria and ER during development, we investigated if PINK1 expression and kinase activity changes in association with autophagy during development. To measure PINK1 levels in flies, we utilized a green fluorescent protein (GFP)-tagged PINK1 that was created by making an in-frame fusion of GFP to the C-terminus of PINK1 (PINK1-GFP) by gene editing[29]. Interestingly, PINK1-GFP is increased 2 hours APF in both male and female intestines compared to respective staged larval controls (Figure S4K–S4L). However, we did not observe significant co-localization of PINK1-GFP with the ER-phagy receptor Rtnl1 (Figure S4M–S4N). Consistent with increased PINK1 levels at the stage when autophagy is induced, phosphorylation of the PINK1 substrate, ubiquitin serine 65, is increased after pupariation compared to larval intestines (Figure 4E and 4F). Furthermore, *Atg8a*$^{\Delta}$ mutant intestines exhibit elevated levels of phosphorylated ubiquitin compared to control intestines after pupariation (Figure 4E and 4F), suggesting that PINK1 is activated during development and autophagy influences phospho-ubiquitin levels. Importantly, *PINK1*^{B9} single mutant and *PINK1*^{B9}*Atg8a*$^{\Delta}$ double mutant intestines lack phosphorylated ubiquitin (Figure 4E and 4F). In addition, *PINK1*^{B9} single mutant intestines possess similar levels of Ref(2)p compared to control intestines after pupariation, and *PINK1*^{B9}*Atg8a*$^{\Delta}$ double mutant intestines possess similar Ref(2)p levels compared to *Atg8a*$^{\Delta}$ single mutant intestines (Figure 4E and 4G).

To investigate if PINK1 regulates ER-phagy through receptors, we tested if Rtnl1 and Atl are altered by *PINK1* loss in enterocytes. Interestingly, *PINK1*^{B9} mutant cells possess decreased Rtnl1–3×Flag-V5 levels (Figure 4H and 4I), and increased Atl-3×Flag-V5 levels (Figure 4J and 4K) compared to neighboring control enterocytes 2 hours APF. Consistent with these data, 28 kDa and 41 kDa Rtnl1 protein levels are decreased in homozygous *PINK1* mutant compared to control intestines 2 hours APF (Figure 4L–4N). A long exposure revealed a high molecular weight Rtnl1 protein smear that was decreased in *PINK1* mutant compared to control intestines (Figure 4L and 4O). In contrast to the decrease in Rtnl1 proteins, Atl is increased in *PINK1* mutant compared to control intestines 2 hours APF (Figure 4L and 4P). These data indicate that PINK1 influences ER-phagy receptor levels.

Parkin has an opposite function from PINK1 in ER clearance

The E3 ubiquitin ligase Parkin is activated by PINK1 to facilitate ubiquitylation of proteins associated with mitochondria during mitophagy[2]. Parkin also functions downstream of PINK1 in *Drosophila*[30,31]. Since the levels of both PINK1 and phosphorylation of its

substrate ubiquitin are elevated during autophagy in the intestine (Figure 4), we tested if Parkin has a similar function to PINK1 in ER-phagy. *Park*$^{\Delta}$ mutant (Figure S5A) intestine enterocytes possess elevated markers of mitochondria, including ATP5A and Mito-GFP, compared to control cells (Figure S5B–S5G). Surprisingly, *Park*$^{\Delta}$ mutant intestine enterocytes exhibit decreased Calnexin intensity and elevated levels of phospho-ubiquitin in the cytoplasm compared to control enterocytes (Figure 5A and 5B, Figure S5D–S5G). Interestingly, *Park*$^{\Delta}$ mutant enterocytes exhibit elevated levels of PINK1 puncta, and more PINK1 puncta co-localize with mitochondria compared to neighboring control cells (Figure S5H and S5I). *Park*$^{\Delta}$ mutant intestine cells also possess similar levels of pan-ubiquitin that localize with mitochondria compared to neighboring control cells (Figure S5J–S5K).

Our data indicate that *Parkin* has the opposite phenotype of *PINK1* in the regulation of ER clearance by autophagy in the intestine. Therefore, investigated how *Parkin* influences the Rtnl1 and Atl ER-phagy receptors. Rtnl1 was localized in more distinct puncta in *Parkin* mutant enterocytes than control cells, and elevated levels of phosphorylated ubiquitin partly co-localize with Rtnl1 in *Parkin* mutant compared to neighboring control enterocytes (Figure 5C–5D). In addition, Rtnl1 co-localization with Atg8a was increased in *Parkin* mutant compared to control intestines at 2 hours APF (Figure 5E–5G). By contrast, Atl appeared similar between *Parkin* mutant and control cells, and also had elevated phosphorylated ubiquitin with increased co-localization with Atl (Figure S5L–S5M). Similarly, *Park*^{25} mutant intestines possess elevated levels of phosphorylated ubiquitin, and similar levels of pan-ubiquitin (Figure 5H–5J). Western blot analysis of ER-phagy receptors revealed that homozygous *Parkin* mutant intestines possess elevated Rtnl1 protein levels while Atl protein levels did not change (Figure 5K–5O). Thus, *Parkin* and *PINK1* mutant intestines possess opposite influences on ER-phagy receptor levels.

We next investigated the influence of *PINK1* and *Parkin* on the content of autophagosomes by TEM. TEM analyses revealed that *PINK1*^{B9} mutant intestine cells exhibit decreased ER-containing autophagosomes and autolysosomes compared to control intestine cells that possess autophagosomes that contain both ER and mitochondria (Figure 5P, 5Q, and 5S). In contrast to *PINK1*^{B9} mutant enterocytes, *Park*^{25} mutant intestine cells possess autophagosomes that contain ER, and are similar to control intestine cells (Figure 5Q–5S). These data reveal that in addition to their previously described functions in mitophagy, PINK1 and Parkin have opposing functions in ER clearance.

PINK1 and Keap1 function in a pathway to regulate ubiquitylation of Rtnl1 and ER-phagy

The distinct ER-phagy phenotypes of *PINK1* and *Parkin* mutant intestine cells prompted us to consider if a different E3 ubiquitin ligase may be required for ER clearance. Kelch-like-ECH-associated-protein 1 (KEAP1) is part of an E3 ubiquitin ligase complex with Cullin3 (Cul3) that is associated with autophagy and the autophagy receptor p62/Ref(2)p[32,33]. Therefore, we tested if Keap1 is required for ER clearance. *Keap1*^{036} mutant intestine enterocytes fail to clear ER, and possess increased Sec61α-GFP intensity and puncta that partially co-localized with Ref(2)p puncta compared to neighboring control cells 2 hours APF (Figure 6A and 6B). Since Keap1 is an adaptor in the Cul3 E3-ubiquitin ligase complex, we tested if Cul3 is required for ER clearance. Similar to *Keap1* mutant cells,

Cul3$^{\Delta}$ mutant enterocytes possess increased Sec61α-GFP compared to control cells 2 hours APF (Figure 6C and 6D).

The Keap1 and Cul3 complex ubiquitylates Nrf2 (Cnc in flies) to target this transcriptional regulator of antioxidant stress response for degradation[34–36]. Consistent with previous studies, the Cnc-regulated antioxidant response element (ARE)-GFP reporter is activated in *Keap1*^{036} mutant intestine enterocytes (Figure S6A–S6B), suggesting that the Keap1-Cul3-Cnc signaling axis is conserved in enterocytes 2 hours APF. In contrast to *Keap1* mutant enterocytes, cells lacking *Cnc* function fail to accumulate the autophagy receptor Ref(2)p (Figure S6C–S6E). Importantly, *Keap1* and *Cnc* double mutant cells fail to modify Calnexin levels compared to *Keap1* single mutant enterocytes (Figure S6F–S6H), suggesting that Keap1-Cul3 regulates ER clearance in a Cnc-independent manner in enterocytes.

We investigated the specificity of Keap1 in the regulation of ER-phagy. Consistent with a role in ER clearance, *Keap1* mutant intestine enterocytes exhibit decreased ER-phagy flux as measured by the ss-pHluorin-mKate2-KDEL-V5 sensor (Figure S6I–S6J). In contrast to the increase in ER-associated Calnexin in *Keap1* mutant enterocytes, Mito-GFP puncta are decreased in *Keap1* mutant compared to neighboring control cells (Figure 6E–6G). Importantly, *Keap1* mutant cells exhibit increased conjugated ubiquitin puncta that co-localize with Ref(2)p puncta, but not with Mito-GFP puncta (Figure S6K–S6L). These data indicate that *Keap1* is required for ER clearance.

Since *Keap1* mutant cells appear to possess fewer mitochondria than control cells, we investigated the impact of Keap1 on mitophagy. We analyzed phospho-ubiquitin (serine 65) and mitochondrial DNA (mtDNA) using an antibody against double strand DNA (dsDNA) in *Keap1* mutant and control intestine cells. Interestingly, *Keap1* mutant cells exhibit decreased mtDNA puncta (dsDNA) that are co-localized with Mito-GFP puncta compared to neighboring control cells (Figure 6H and 6I). Importantly, this decrease in mtDNA puncta in *Keap1* mutant cells is suppressed by loss of *Atg16* function (Figure S6M–S6N). In addition, *Keap1* mutant cells possess increased co-localization of phospho-ubiquitin puncta and Mito-GFP puncta compared to control cells (Figure 6H and 6J).

PINK1 and *Keap1* mutant intestine cells possess similar defects in ER clearance. Therefore, we investigated the influence of Keap1 on ER-phagy receptors. Consistent with *PINK1* mutants, *Keap1* mutant enterocytes possess reduced Rtnl1 levels compared to control cells 2 hours APF (Figure 6K and 6L). In addition, *Keap1* RNAi knockdown cells exhibit slightly increased Atl levels compared to neighboring control enterocytes (Figure 6M and 6N). Western blot analysis also revealed decreased Rtnl1 and increased Atl protein levels in intestines with reduced *Keap1* function (Figure 6O–6S).

We next examined the relationship between PINK1 and Keap1 by measuring ER-phagy flux using the ss-pHluorin-mKate2-KDEL-V5 sensor in *Keap1* knockdown and *PINK1* mutant intestines. Either *Keap1* knockdown or homozygous *PINK1*^{B9} mutant intestines exhibit a comparable decrease in ER-phagy flux (Figure 7A–7C, and 7E). Significantly, intestines that express *Keap1* RNAi in homozygous *PINK1*^{B9} mutant animals possess a similar decrease in ER-phagy flux compared to either *Keap1* knockdown or *PINK1* mutant intestines alone

(Figure 7D and 7E). These data suggest that Keap1 and PINK1 are in the same pathway to regulate ER clearance.

To investigate how PINK1 and Parkin influence Keap1, we created tagged Keap1–3×Flag-V5 *Drosophila* by CRISPR-Cas9 gene editing (Figure S7A). In *Atg9* mutant enterocytes, Keap1 levels are slightly increased and co-localize with mitochondrial ATP5A puncta (Figure S7B–S7C). Interestingly, *PINK1* mutant enterocytes possess enlarged Keap1 puncta that co-localize with mitochondrial ATP5A (Figure 7F and 7G). Although *Parkin* mutant enterocytes also possess elevated mitochondrial ATP5A, Keap1 levels are similar and mitochondria exhibit less co-localization with Keap1 compared to *PINK1* mutant cells (Figure 7H and 7I). Furthermore, *Parkin* mutant cells possess increased co-localization of Keap1 with phosphorylated ubiquitin (Figure S7D–S7E). Although Keap1 protein is present in both *PINK1* and *Parkin* mutant intestines, Keap1 is elevated in *PINK1* mutants compared to both control and *Parkin* mutant intestines (Figure 7J and 7K). These data indicate that PINK1 influences Keap1 mitochondrial localization, and that Parkin is not required for Keap1 proximity with mitochondria.

PINK1 and *Keap1* mutant cells have similar defects in ER clearance, as well as similar influences on Rtnl1 and Atl ER-phagy receptor levels. Interestingly, *Parkin* mutants possess opposite phenotypes to both *PINK1* and *Keap1*. Given the high molecular weight Rtnl1 protein smear that was changed in PINK1, Parkin and Keap1 deficient intestines (Figure 4L and 4O, Figure 5J and 5M, and Figure 6O and 6R), we examined if this may reflect ubiquitylation of Rtnl1. Intestines were dissected from staged animals, followed by immunoprecipitation of Rtnl1, and immunoblotting for ubiquitin. Loss of *PINK1* results in decreased ubiquitylation of Rtnl1 (Figure 7L and 7M). By contrast, *Parkin* mutant intestines possess increased Rtnl1 ubiquitylation compared to control intestines (Figure 7N and 7O). Consistent with *PINK1*, *Keap1* knockdown intestines possess decreased Rtnl1 ubiquitylation compared to control intestines (Figure 7P and 7Q). These data indicate that PINK1 and Keap1 are required for Rtnl1 ubiquitylation, and that Parkin negatively regulates Rtnl1 ubiquitylation. Together, our data indicate that PINK1 regulates the clearance of ER and mitochondria by autophagy, and that Keap1 is required for ER-phagy while Parkin regulates mitophagy.

DISCUSSION

The ER provides membranes to form different vesicles, including autophagosomes[37]. In addition, ER contacts multiple organelles[38], raising complexity in understanding how organelle relationships influence cell quality control. Mitochondria and ER are selectively removed by utilizing distinct proteins during intestine development. Specifically, the mitophagy receptor BNIP3 regulates mitochondria clearance, and the ER-phagy receptors Trp1, Atl and Rtnl1 regulate ER clearance.

PINK1 is a mitochondrial protein that phosphorylates ubiquitin to promote the recruitment of mitophagy components to mitochondria, including Parkin[2]. Interestingly, our data indicates that PINK1 is required for ER clearance. In contrast to *PINK1* mutant cells that fail to clear ER, *Parkin* mutant cells possess decreased ER, and increased phosphorylated

ubiquitin. Parkin is known to facilitate ubiquitylation of mitochondrial proteins during mitophagy[2]. Thus, Parkin influences the localization of PINK1-dependent phosphorylated ubiquitin to influence selective organelle clearance.

Cells lacking the E3 ubiquitin ligase component Keap1 have the same defect in ER-phagy as *PINK1* mutant cells. In contrast to *Parkin* mutant cells that fail to clear mitochondria and have decreased ER, *Keap1* mutant intestine cells fail to clear ER and possess decreased mitochondria. These opposing phenotypes indicate that PINK1 functions in divergent pathways to clear ER and mitochondria, with Keap1 regulating ER-phagy and Parkin controlling mitophagy. PINK1 is localized to mitochondria where it phosphorylates ubiquitin to regulate mitophagy[39]. Thus, inter-organelle communication influences cargoe selection for autophagy. In contrast to the Keap1, Cul3 and Nrf2 pathway that modulates autophagy and antioxidant stress response[32,36], the Keap1 and Cul3 E3 complex facilitates ER-phagy and inhibits mitophagy during developmental organelle clearance in the fly intestine. PINK1 functions upstream of Keap1, and *PINK1* and *Keap1* have similar influence on Rtnl1 and Atl ER-phagy receptors. Both *PINK1* and *Keap1* are required for ubiquitylation of Rtnl1. In addition, Keap1 is enriched near mitochondria in *PINK1* mutant cells. Therefore, PINK1 influences distinct E3 ubiquitin ligases to specify clearance of ER and mitochondria.

The roles of mitophagy receptor ubiquitylation are clear, but less is known about ubiquitin and ER-phagy receptors. Two recent studies indicate that ubiquitin plays an important role in ER-phagy[40,41]. Our data indicate that phospho-ubiquitin partly localized with Rtnl1 in *Parkin* mutant compared to control cells. Since *Parkin* mutant cells possess increased ER clearance, these data suggest that phospho-ubiquitin association with Rtnl1 contributes to ER-phagy. ER-phagy receptors are resident ER proteins that bind to Atg8/LC3, and influence ER shape[42,43]. Multiple ER-phagy receptors are required for ER clearance. Interestingly, *Rtnl1* and *Atl* mutant intestine cells manifest different ER morphologies. In addition, *PINK1* and *Keap1* mutant cells possess the same decrease in Rtnl1 and increase in Atl, while *Atl* mutant cells fail to clear Rtnl1. These data suggest that ubiquitylation of receptors influences their levels, and this could influence ER shape needed for ER-phagy.

In summary, ER is selectively degraded during developmental autophagy. This physiological model reveals that clearance of ER and mitochondria requires common autophagy machinery, as well as organelle-specific receptors within a single cell. Significantly, PINK1 is required for clearance of both ER and mitochondria. By contrast, Keap1 and Parkin possess opposing roles in the clearance of ER and mitochondria downstream of PINK1. These studies reveal that much remains to be learned about how a cell determines how much and which autophagic substrates are cleared, and the impact of these selective autophagy programs on health and disease.

Limitations of the study

Further investigations are needed to understand if PINK1, Keap1 and Cul3 regulate ER-phagy in other cell contexts, including human cells. It is also important to discover other cell contexts where ER-phagy is a normal physiological response. Mechanistic issues need to be resolved, including how PINK1 kinase function regulates Keap1 and Cul3 ubiquitylation of

Rtnl1. Finally, it is critical to resolve the relationships between the ER-phagy receptors, and determine how their ubiquitylation influences ER shape and ER-phagy.

STAR★METHODS

RESOURCE AVAILABILITY

Lead contact—Further information and requests for resources and reagents should be directed to and will be fulfilled by the lead contact: Eric H. Baehrecke (eric.baehrecke@umassmed.edu).

Materials availability—Plasmids, *Drosophila* lines and datasets generated in this study are available on request from the lead contact.

Data and code availability

- Microscopy data and original western blot images reported in this paper will be shared by the lead contact upon request.
- No original code was used in this study.
- Any additional information required to reanalyze the data in this paper is available from the lead contact upon request.

EXPERIMENTAL MODEL AND STUDY PARTICIPANT DETAILS

Drosophila melanogaster strains used in this study are listed in the KEY RESOURCES TABLE. All *Drosophila* genotypes are provided (Table S1). The animals used in this study were of both genders unless noted for specific mutant genotypes. Animals were analyzed as either feeding third instar larvae or 2 hours after puparium formation as noted. We did not observe any influence of gender on results. Flies were reared at 25 °C on standard cornmeal/molasses/agar media.

METHOD DETAILS

Fly stocks—Flies were reared at 25 °C on standard cornmeal-molasses-agar media. PINK1-GFP was a gift from Hong Xu[29]. $Atg9^{D51}$ was a gift from G. Chen[44]. $Vps34^{m22}$ was a gift from Thomas Neufeld[45]. Alt^{2} [46] and $Rtnl1^{1W}$ [47] were gifts from James McNew. $Park^{25}$ [48] were gifts from Leo Pallanck. $PINK1^{B9}$ was a gift from Jongkyeong Chung[30]. $PINK1^{5}$ was a gift from Ming Guo[31]. $Keap1^{036}$ was a gift from Dirk Bohmann[36]. Cnc^{1223} was a gift from Fengwei Yu[49].

To generate UAS-ss-Rtnl1-pHluorin-mKate2-KDEL-V5, the coding region flanked by 15 bp homologous arms (Table S2) was synthesized by IDT (San Diego, California) and assembled into a pUAST-attB vector using the In-Fusion HD Cloning Kit (Takara, 639650). Plasmid DNA was injected by Bestgene (Chino Hills, California) into a strain carrying either attP40 or attP2 landing sites, and integrated into either the second or the third chromosome of the *Drosophila* genome using phiC31 integrase.

The *Atg8a* loss-of-function mutant $Atg8a^{\Delta}$ strain was created using the CRISPR/Cas9 gene editing[50]. sgRNA targeting sequences are provided (Table S2). A 0.8 kb gblock flanking the region of deletion was synthesized by IDT (San Diego, California) and inserted into a TOPO vector (Invitrogen, 450641). gRNAs and donors were co-injected into vasa-Cas9 transgenic flies with different chromosome of Cas9 insertion against target gene localized chromosome. Germline injection was done by Bestgene (Chino Hills, California). Progeny were collected and screened for *Atg8a* deletion by DNA sequencing.

The Parkin loss-of-function $Park^{\Delta}$ FRT2A strain was created by crossing *vas-Cas9*; FRT2A with *Park* gRNA transgenic flies (gRNA sequence provided in Table S2). The BNIP3 loss-of-function $BNIP3^{\Delta}$ strain was generated by crossing *vas-Cas9* with *BNIP3* dual-gRNA transgenic flies (gRNA sequence provided in (Table S2). Progeny were collected and screened for deletion by DNA sequencing (sequencing primers provided in Table S2).

Gene editing to tag Rtnl1, Atl and Keap1—*Rtnl1*, *Atl* and *Keap1* encoded proteins were tagged on their C-termini with 3×Flag-V5 separated by a 15 amino acids poly-glycine peptide linker (GGGGSGLRSSRGPFE) by CRISPR-Cas9 gene editing. gRNAs were designed by https://flycrispr.org/ and https://www.flyrnai.org/crispr3/web/ with low off-target score and high frame shift score and selected against off-targeting on the gene located chromosome. We used two gRNAs flanking the Rtnl1 stop codon, one gRNA proximal to the Atl stop codon and two gRNAs flanking the Keap1 stop codon for gene editing. gRNA oligonucleotides were synthesized by IDT and subcloned into pCFD2-dU6:3 gRNA (Addgene). Related guide RNA sequences are provided in Table S2. We designed 600–800 bp homologous arms for each gene and all PAM sequences were silent mutations unless the PAM was located in the intron or 3'-UTR regions. Homologous directed repair donor templates were synthesized by IDT and subcloned into TOPO vectors (Invitrogen). gBlock sequences are provided in Table S2. gRNAs and donors were co-injected into vasa-Cas9 transgenic flies with a different chromosome of Cas9 insertion against target gene located chromosome. Germline injection was conducted by Bestgene (Chino Hills, California). Progeny were collected and screened for precise insertions by DNA sequencing.

Induction of mosaic RNAi/mutant cell clones and whole intestine RNAi expression—Mosaic dsRed positive RNAi- and transgene-expressing cell clones and fluorescent-negative cell clones were induced as described[23]. To induce RNAi-expressing cell clones in the intestine, virgin female hsFlp;; Sec61α-GFP, Act>CD2>GAL4, UAS-dsRed were crossed with RNAi line males. One-day-old eggs were heat shocked at 37 °C for 5 minutes. To induce $BNIP3^{wko}$ CRISPR mutant cell clones the midgut, virgin female hsFlp; UAS-Cas9; Sec61α-GFP, Act>CD2>GAL4, UAS-dsRed were crossed with male $BNIP3^{wko}$. One-day-old eggs were heat shocked at 37 °C for 15 minutes. To induce loss-of-function cell clones, 0–4 hour-old embryos were heat shocked at 37 °C for 1 hour. Myo31DFNP0001 (NP1-GAL4) was used to drive RNAi expression in the whole intestine.

Protein expression and purification—The coding regions of *Drosophila Atl*, *Rtnl1*, *Trp1* and *Atg8a* cDNAs from clones GH09383, LD14068, RE23984 and LD05816 (*Drosophila* Genomics Resource Center, Bloomington, IN, USA) were amplified using Q5 High-Fidelity DNA Polymerase (NEB, M0492S) with primers in Table S2, and subcloned

into pMAL-c5X (NEB N8108S) MBP and pGEX-6P-2 GST (GE Healthcare Life Sciences) expression vectors. Mutations in putative LC3/GABARAP/Atg8a interacting regions (LIR) of Atl (EAGRA), Trp1 (AAVWA, DAEIA, EALDA) that were predicted by software (https://ilir.warwick.ac.uk/search.php) were mutated with primers in Table S2 using Q5 Site-Directed Mutagenesis Kit (NEB, E0554S) so that two essential amino acids were replaced by alanine. MBP alone, MBP-Atl and LIR mutant ATL, MBP-Rtnl1, MBP-Trp1 and LIR mutant Trp1, and GST-Atg8a were expressed in *E. coli* BL21, immobilized with either MBP magnetic beads (NEB, E8037S) or Glutathione magnetic beads in binding (20 mM Tris-HCl, pH 7.5, 10 mM EDTA, 5 mM EGTA, 150 mM NaCl, 0.1 % β-ME, protease inhibitor cocktail) and wash buffer (1% Triton-X100, 20 mM Tris-HCl, pH 7.5, 10 mM EDTA, 5 mM EGTA, 150 mM NaCl, 0.1 % β-ME, protease inhibitor cocktail). MBP tagged proteins were eluted in maltose elution buffer (10 mM maltose, 20 mM Tris-HCl, pH 7.5), and GST-Atg8a was eluted in glutathione elution buffer (10 mM glutathione, 20 mM Tris-HCl, pH 7.5).

Atg8a binding assay—20 μg of GST-Atg8a protein was immobilized onto glutathione magnetic beads in Atg8a binding buffer (20 mM Tris-HCl, pH 7.5, 10 mM EDTA, 5 mM EGTA, 150 mM NaCl, 0.1 % β-ME, protease inhibitor cocktail) for 30 minutes at 4 °C. Atg8a binding beads were then incubated with 20 μg MBP-Rtnl1, MBP-Atl, MBP-Trp1 and relatives containing putative LIR mutant proteins for 2 hours at 4 °C. The beads were washed 6 times with wash buffer (1% Triton-X100, 20 mM Tris-HCl, pH 7.5, 10 mM EDTA, 5 mM EGTA, 150 mM NaCl, 0.1 % β-ME, protease inhibitor cocktail) and resuspended in 2xLaemli sample buffer. The samples were separated using 4%−20% SDS-PAGE, transferred, and antibody against MBP (HRP conjugated, 1:20000, NEB, E8038) was used to detect MBP-fusion proteins. Atg8a was detected using antibody against GABARAP (1:1000, Cell signaling, 13733).

Immunolabeling and microscopy—Intestines were dissected from staged animals in PBS, fixed with 4% paraformaldehyde (PFA) in PBS 0.3% Triton X-100 (PBST), and blocked with goat serum for 2 hours before incubating with primary antibodies in 0.3% PBST with 5% goat serum. We used mouse anti-Calnexin (1:100), rabbit anti-Ref(2)p/p62 (1:200), mouse anti-ATP5A (1:200), mouse anti-dsDNA (1:40), rabbit anti-phospho-ubiquitin (serine 65, 1:200, E5T1W), mouse anti-ubiquitin (1:200, P4D1), mouse anti-conjugated ubiquitin (1:200, UBCJ2), mouse anti-GFP (1:200), mouse anti-V5 (1:200), rabbit anti-V5 (1:200), and rabbit anti-FLAG (1:200) for immunostaining. All secondary antibodies (1:200) were incubated for 2 hours at room temperature. Hoechst 33342 dye was used to stain DNA. Tissues were mounted in VectaShield.

Samples were imaged using a Zeiss LSM 700 confocal microscope equipped with a Plan-Apochromat 63x/1.40 Oil DIC M27 objective using Zeiss Zen Software and a Nikon A1R HD25 confocal microscope equipped with a CFI Plan Apochromat 60x/1.4 Oil DIC objective NIS-Elements Viewer software. Images collected with the Nikon confocal microscope were further magnified by 2.88. Images were deconvoluted using NIS-Elements C software and processed with Fiji[51].

LysoTracker staining—Fly intestines expressing the Rtnl1-pHluorin-mKate2 sensor were dissected 2 hours after pupariation in PBS, and incubated with LysoTracker Deep Red

(1:300, Invitrogen, L12492) and Hoechst 33342 DNA stain (1:100) in PBS at room temperature for 10–15 minutes. Intestines were mounted in VectaShield and immediately imaged by confocal microscopy.

Immunoblotting and immunoprecipitation—Intestines from 20 staged *Drosophila* were dissected 2 hours after puparium formation in prechilled PBS for each genotype, including those expressing RNAis and UAS-ss-pHluorin-mKate2-KDEL-V5 driven by NP1-GAL4, homozygous mutants, and respective controls, and homogenized in 2xSDS sample buffer (2% SDS, 63 mM Tris-HCl, pH 6.8, 10% glycerol) supplemented with protease and phosphatase inhibitor cocktail and 1 mM PMSF. 20 μg of protein measured by BCA protein assay from each genotype lysate was mixed with LDS sample buffer analyzed by western and immunoblotted with mouse anti-Calnexin (1:1000), rabbit anti-Ref(2)p (1:1000), rabbit anti-phospho-ubiquitin (serine 65, 1:1000, E2J6T), mouse anti-ubiquitin (1:1000, P4D1), mouse anti-V5 (1:2000), mouse anti-GFP (1:2000) and mouse anti-Actin (1:1000) antibodies.

For immunoprecipitation experiments, intestines from 70–90 staged *Drosophila* were dissected 2 hours APF in prechilled PBS for each genotype. A subgroup of 20–30 intestines of each genotype were ground in 40 μl prechilled freshly made co-immunoprecipitation (COIP) buffer (1% Triton X-100, 10 mM HEPES, pH 7.5, 142.5 mM KCl, 5 mM $MgCl_2$,1 mM EDTA, 10% glycerol) supplemented with protease and phosphatase inhibitor cocktail and 1 mM PMSF. All subgroup lysates of each genotype were placed on ice until dissection was completed, and then merged and supplemented with COIP buffer to 500 μl for an extra 1 hour of incubation at 4 °C with rotation. 15–20 μl of total lysates (input) were collected and mixed with LDS sample buffer followed by boiling. 600–700 mg proteins of each genotype as determined by BCA protein assay were incubated with 20 μl of V5-Trap agarose beads supplemented with COIP buffer to 1 ml at 4 °C overnight with rotation. Agarose beads were washed 5 times with COIP buffer for 20 minutes at 4 °C with rotation and eluted with LDS sample buffer followed by boiling. Both input lysates and immunoprecipitated lysates were analyzed by western and immunoblotted with mouse anti-ubiquitin (P4D1, 1:1000), mouse anti-V5 (1:1000), rabbit anti-V5 (1:1000) and mouse anti-Actin (1:1000) antibodies.

Transmission electron microscopy—As previously described[23], intestines were dissected in PBS 2 hours after pupariation, fixed over night at 4°C in a solution of 2.5% glutaraldehyde and 2% paraformaldehyde in 0.1 M sodium cacodylate buffer, pH 7.4, osmicated, and washed in distilled water. Preparations were stained en bloc in 1% aqueous uranyl acetate and dehydrated through a graded ethanol series, treated with propylene oxide and infiltrated in SIP-pon/Araldite for embedding. Ultrathin sections of the anterior region of the midgut were collected and stained with uranyl acetate and lead citrate. For each genotype, at least 3 intestines were embedded and sectioned for analyses and quantification. Imaging was performed using a Phillips CM10 TEM.

QUANTIFICATION AND STATISTICAL ANALYSIS

Fiji[51] was used to quantify immunofluorescence intensity and puncta in images. Fiji and Image Studio Lite were used to quantify protein levels in western blot analyses. p-values were calculated using either a two-tailed unpaired t-test, Kruskal-Wallis H test or One-Way ANOVA corrected by Tukey's post-hoc test or Fisher's LSD test from Graphpad Prism 5 (https://www.graphpad.com/scientific-software/prism/). The number (n) of samples analyzed by immunostaining represents number of enterocytes cells from at least 4 independent animals from each genotype. No animals were excluded from statistical analyses, the experiments were not randomized, and the investigators were not blinded. All error bars are SEM.

Supplementary Material

Refer to Web version on PubMed Central for supplementary material.

ACKNOWLEDGEMENTS

We thank F. Yu, G. Chen, H. Xu, J.A. McNew, L.J. Pallanck, Vienna *Drosophila* Resource Center, Bloomington *Drosophila* stock center, and Kyoto *Drosophila* Genetic Resource Center for flies, the Electron Microscopy Core Facility at UMass Chan Medical School, and I. Dikic, F. Kraus and J.W. Harper for advice. This work was supported by R35GM131689 to E.H.B and F30CA239374 to J.L.S..

REFERENCES

1. Hubner CA, and Dikic I (2020). ER-phagy and human diseases. Cell Death Differ 27, 833–842. 10.1038/s41418-019-0444-0. [PubMed: 31659280]
2. Pickles S, Vigie P, and Youle RJ (2018). Mitophagy and Quality Control Mechanisms in Mitochondrial Maintenance. Curr Biol 28, R170–R185. 10.1016/j.cub.2018.01.004. [PubMed: 29462587]
3. Jin SM, Lazarou M, Wang C, Kane LA, Narendra DP, and Youle RJ (2010). Mitochondrial membrane potential regulates PINK1 import and proteolytic destabilization by PARL. J Cell Biol 191, 933–942. 10.1083/jcb.201008084. [PubMed: 21115803]
4. Kim Y, Park J, Kim S, Song S, Kwon SK, Lee SH, Kitada T, Kim JM, and Chung J (2008). PINK1 controls mitochondrial localization of Parkin through direct phosphorylation. Biochem Biophys Res Commun 377, 975–980. 10.1016/j.bbrc.2008.10.104. [PubMed: 18957282]
5. Shiba-Fukushima K, Imai Y, Yoshida S, Ishihama Y, Kanao T, Sato S, and Hattori N (2012). PINK1-mediated phosphorylation of the Parkin ubiquitin-like domain primes mitochondrial translocation of Parkin and regulates mitophagy. Sci Rep 2, 1002. 10.1038/srep01002. [PubMed: 23256036]
6. Ordureau A, Sarraf SA, Duda DM, Heo JM, Jedrychowski MP, Sviderskiy VO, Olszewski JL, Koerber JT, Xie T, Beausoleil SA, et al. (2014). Quantitative proteomics reveal a feedforward mechanism for mitochondrial PARKIN translocation and ubiquitin chain synthesis. Mol Cell 56, 360–375. 10.1016/j.molcel.2014.09.007. [PubMed: 25284222]
7. Koyano F, Okatsu K, Kosako H, Tamura Y, Go E, Kimura M, Kimura Y, Tsuchiya H, Yoshihara H, Hirokawa T, et al. (2014). Ubiquitin is phosphorylated by PINK1 to activate parkin. Nature 510, 162–166. 10.1038/nature13392. [PubMed: 24784582]
8. Wauer T, Simicek M, Schubert A, and Komander D (2015). Mechanism of phosphoubiquitin-induced PARKIN activation. Nature 524, 370–374. 10.1038/nature14879. [PubMed: 26161729]
9. Kane LA, Lazarou M, Fogel AI, Li Y, Yamano K, Sarraf SA, Banerjee S, and Youle RJ (2014). PINK1 phosphorylates ubiquitin to activate Parkin E3 ubiquitin ligase activity. J Cell Biol 205, 143–153. 10.1083/jcb.201402104. [PubMed: 24751536]

10. Lazarou M, Sliter DA, Kane LA, Sarraf SA, Wang C, Burman JL, Sideris DP, Fogel AI, and Youle RJ (2015). The ubiquitin kinase PINK1 recruits autophagy receptors to induce mitophagy. Nature 524, 309–314. 10.1038/nature14893. [PubMed: 26266977]
11. Abudu YP, Shrestha BK, Zhang W, Palara A, Brenne HB, Larsen KB, Wolfson DL, Dumitriu G, Oie CI, Ahluwalia BS, et al. (2021). SAMM50 acts with p62 in piecemeal basal- and OXPHOS-induced mitophagy of SAM and MICOS components. J Cell Biol 220. 10.1083/jcb.202009092.
12. Khaminets A, Heinrich T, Mari M, Grumati P, Huebner AK, Akutsu M, Liebmann L, Stolz A, Nietzsche S, Koch N, et al. (2015). Regulation of endoplasmic reticulum turnover by selective autophagy. Nature 522, 354–358. 10.1038/nature14498. [PubMed: 26040720]
13. Mochida K, Oikawa Y, Kimura Y, Kirisako H, Hirano H, Ohsumi Y, and Nakatogawa H (2015). Receptor-mediated selective autophagy degrades the endoplasmic reticulum and the nucleus. Nature 522, 359–362. 10.1038/nature14506. [PubMed: 26040717]
14. Fumagalli F, Noack J, Bergmann TJ, Cebollero E, Pisoni GB, Fasana E, Fregno I, Galli C, Loi M, Solda T, et al. (2016). Translocon component Sec62 acts in endoplasmic reticulum turnover during stress recovery. Nat Cell Biol 18, 1173–1184. 10.1038/ncb3423. [PubMed: 27749824]
15. Grumati P, Morozzi G, Holper S, Mari M, Harwardt MI, Yan R, Muller S, Reggiori F, Heilemann M, and Dikic I (2017). Full length RTN3 regulates turnover of tubular endoplasmic reticulum via selective autophagy. Elife 6. 10.7554/eLife.25555.
16. Chino H, Hatta T, Natsume T, and Mizushima N (2019). Intrinsically Disordered Protein TEX264 Mediates ER-phagy. Mol Cell 74, 909–921 e906. 10.1016/j.molcel.2019.03.033. [PubMed: 31006538]
17. Chen Q, Xiao Y, Chai P, Zheng P, Teng J, and Chen J (2019). ATL3 Is a Tubular ER-Phagy Receptor for GABARAP-Mediated Selective Autophagy. Curr Biol 29, 846–855 e846. 10.1016/j.cub.2019.01.041. [PubMed: 30773365]
18. Liang JR, Lingeman E, Ahmed S, and Corn JE (2018). Atlastins remodel the endoplasmic reticulum for selective autophagy. J Cell Biol 217, 3354–3367. 10.1083/jcb.201804185. [PubMed: 30143524]
19. Nthiga TM, Kumar Shrestha B, Sjottem E, Bruun JA, Bowitz Larsen K, Bhujabal Z, Lamark T, and Johansen T (2020). CALCOCO1 acts with VAMP-associated proteins to mediate ER-phagy. EMBO J 39, e103649. 10.15252/embj.2019103649. [PubMed: 32525583]
20. Chang TK, Shravage BV, Hayes SD, Powers CM, Simin RT, Wade Harper J, and Baehrecke EH (2013). Uba1 functions in Atg7- and Atg3-independent autophagy. Nat Cell Biol 15, 1067–1078. 10.1038/ncb2804. [PubMed: 23873149]
21. Shen JL, Fortier TM, Wang R, and Baehrecke EH (2021). Vps13D functions in a Pink1-dependent and Parkin-independent mitophagy pathway. J Cell Biol 220. 10.1083/jcb.202104073.
22. Hu Y, Flockhart I, Vinayagam A, Bergwitz C, Berger B, Perrimon N, and Mohr SE (2011). An integrative approach to ortholog prediction for disease-focused and other functional studies. BMC Bioinformatics 12, 357. 10.1186/1471-2105-12-357. [PubMed: 21880147]
23. Anding AL, Wang C, Chang TK, Sliter DA, Powers CM, Hofmann K, Youle RJ, and Baehrecke EH (2018). Vps13D Encodes a Ubiquitin-Binding Protein that Is Required for the Regulation of Mitochondrial Size and Clearance. Curr Biol 28, 287295.e286. 10.1016/j.cub.2017.11.064.
24. Shen JL, Fortier TM, Zhao YG, Wang R, Burmeister M, and Baehrecke EH (2021). Vmp1, Vps13D, and Marf/Mfn2 function in a conserved pathway to regulate mitochondria and ER contact in development and disease. Curr Biol. 10.1016/j.cub.2021.04.062.
25. Wang R, Miao G, Shen JL, Fortier TM, and Baehrecke EH (2022). ESCRT dysfunction compromises endoplasmic reticulum maturation and autophagosome biogenesis in Drosophila. Curr Biol 32, 1262–1274 e1264. 10.1016/j.cub.2022.01.040. [PubMed: 35134326]
26. Novak I, Kirkin V, McEwan DG, Zhang J, Wild P, Rozenknop A, Rogov V, Lohr F, Popovic D, Occhipinti A, et al. (2010). Nix is a selective autophagy receptor for mitochondrial clearance. EMBO Rep 11, 45–51. 10.1038/embor.2009.256. [PubMed: 20010802]
27. Ordureau A, Kraus F, Zhang J, An H, Park S, Ahfeldt T, Paulo JA, and Harper JW (2021). Temporal proteomics during neurogenesis reveals large-scale proteome and organelle remodeling via selective autophagy. Mol Cell 81, 5082–5098 e5011. 10.1016/j.molcel.2021.10.001. [PubMed: 34699746]

28. Zhang T, Xue L, Li L, Tang C, Wan Z, Wang R, Tan J, Tan Y, Han H, Tian R, et al. (2016). BNIP3 Protein Suppresses PINK1 Kinase Proteolytic Cleavage to Promote Mitophagy. Journal of Biological Chemistry 291, 21616–21629. 10.1074/jbc.M116.733410. [PubMed: 27528605]
29. Zhang Y, Wang ZH, Liu Y, Chen Y, Sun N, Gucek M, Zhang F, and Xu H (2019). PINK1 Inhibits Local Protein Synthesis to Limit Transmission of Deleterious Mitochondrial DNA Mutations. Mol Cell 73, 1127–1137 e1125. 10.1016/j.molcel.2019.01.013. [PubMed: 30772175]
30. Park J, Lee SB, Lee S, Kim Y, Song S, Kim S, Bae E, Kim J, Shong M, Kim JM, and Chung J (2006). Mitochondrial dysfunction in Drosophila PINK1 mutants is complemented by parkin. Nature 441, 1157–1161. 10.1038/nature04788. [PubMed: 16672980]
31. Clark IE, Dodson MW, Jiang C, Cao JH, Huh JR, Seol JH, Yoo SJ, Hay BA, and Guo M (2006). Drosophila pink1 is required for mitochondrial function and interacts genetically with parkin. Nature 441, 1162–1166. 10.1038/nature04779. [PubMed: 16672981]
32. Komatsu M, Kurokawa H, Waguri S, Taguchi K, Kobayashi A, Ichimura Y, Sou YS, Ueno I, Sakamoto A, Tong KI, et al. (2010). The selective autophagy substrate p62 activates the stress responsive transcription factor Nrf2 through inactivation of Keap1. Nat Cell Biol 12, 213–223. 10.1038/ncb2021. [PubMed: 20173742]
33. Taguchi K, Fujikawa N, Komatsu M, Ishii T, Unno M, Akaike T, Motohashi H, and Yamamoto M (2012). Keap1 degradation by autophagy for the maintenance of redox homeostasis. Proc Natl Acad Sci U S A 109, 13561–13566. 10.1073/pnas.1121572109. [PubMed: 22872865]
34. Kobayashi A, Kang MI, Okawa H, Ohtsuji M, Zenke Y, Chiba T, Igarashi K, and Yamamoto M (2004). Oxidative stress sensor Keap1 functions as an adaptor for Cul3based E3 ligase to regulate proteasomal degradation of Nrf2. Mol Cell Biol 24, 71307139. 10.1128/MCB.24.16.7130-7139.2004.
35. Zhang DD, Lo SC, Cross JV, Templeton DJ, and Hannink M (2004). Keap1 is a redox-regulated substrate adaptor protein for a Cul3-dependent ubiquitin ligase complex. Mol Cell Biol 24, 10941–10953. 10.1128/MCB.24.24.10941-10953.2004. [PubMed: 15572695]
36. Sykiotis GP, and Bohmann D (2008). Keap1/Nrf2 signaling regulates oxidative stress tolerance and lifespan in Drosophila. Dev Cell 14, 76–85. 10.1016/j.devcel.2007.12.002. [PubMed: 18194654]
37. Tooze SA, and Yoshimori T (2010). The origin of the autophagosomal membrane. Nat Cell Biol 12, 831–835. 10.1038/ncb0910-831. [PubMed: 20811355]
38. Phillips MJ, and Voeltz GK (2016). Structure and function of ER membrane contact sites with other organelles. Nat Rev Mol Cell Biol 17, 69–82. 10.1038/nrm.2015.8. [PubMed: 26627931]
39. Pickrell AM, and Youle RJ (2015). The roles of PINK1, parkin, and mitochondrial fidelity in Parkinson's disease. Neuron 85, 257–273. 10.1016/j.neuron.2014.12.007. [PubMed: 25611507]
40. Gonzalez A, Covarrubias-Pinto A, Bhaskara RM, Glogger M, Kuncha SK, Xavier A, Seemann E, Misra M, Hoffmann ME, Brauning B, et al. (2023). Ubiquitination regulates ER-phagy and remodelling of endoplasmic reticulum. Nature 618, 394–401. 10.1038/s41586-023-06089-2. [PubMed: 37225996]
41. Foronda H, Fu Y, Covarrubias-Pinto A, Bocker HT, Gonzalez A, Seemann E, Franzka P, Bock A, Bhaskara RM, Liebmann L, et al. (2023). Heteromeric clusters of ubiquitinated ER-shaping proteins drive ER-phagy. Nature 618, 402–410. 10.1038/s41586-023-06090-9. [PubMed: 37225994]
42. Shibata Y, Hu J, Kozlov MM, and Rapoport TA (2009). Mechanisms shaping the membranes of cellular organelles. Annu Rev Cell Dev Biol 25, 329–354. 10.1146/annurev.cellbio.042308.113324. [PubMed: 19575675]
43. Gubas A, and Dikic I (2022). ER remodeling via ER-phagy. Mol Cell 82, 1492–1500. 10.1016/j.molcel.2022.02.018. [PubMed: 35452617]
44. Wen JK, Wang YT, Chan CC, Hsieh CW, Liao HM, Hung CC, and Chen GC (2017). Atg9 antagonizes TOR signaling to regulate intestinal cell growth and epithelial homeostasis in Drosophila. Elife 6. 10.7554/eLife.29338.
45. Juhasz G, Hill JH, Yan Y, Sass M, Baehrecke EH, Backer JM, and Neufeld TP (2008). The class III PI(3)K Vps34 promotes autophagy and endocytosis but not TOR signaling in Drosophila. J Cell Biol 181, 655–666. 10.1083/jcb.200712051. [PubMed: 18474623]

46. Lee M, Paik SK, Lee MJ, Kim YJ, Kim S, Nahm M, Oh SJ, Kim HM, Yim J, Lee CJ, et al. (2009). Drosophila Atlastin regulates the stability of muscle microtubules and is required for synapse development. Dev Biol 330, 250–262. 10.1016/j.ydbio.2009.03.019. [PubMed: 19341724]

47. Wakefield S, and Tear G (2006). The Drosophila reticulon, Rtnl-1, has multiple differentially expressed isoforms that are associated with a sub-compartment of the endoplasmic reticulum. Cell Mol Life Sci 63, 2027–2038. 10.1007/s00018-006-6142-3. [PubMed: 16847576]

48. Greene JC, Whitworth AJ, Kuo I, Andrews LA, Feany MB, and Pallanck LJ (2003). Mitochondrial pathology and apoptotic muscle degeneration in Drosophila parkin mutants. Proc Natl Acad Sci U S A 100, 4078–4083. 10.1073/pnas.0737556100. [PubMed: 12642658]

49. Chew LY, Zhang H, He J, and Yu F (2021). The Nrf2-Keap1 pathway is activated by steroid hormone signaling to govern neuronal remodeling. Cell Rep 36, 109466. 10.1016/j.celrep.2021.109466. [PubMed: 34348164]

50. Gratz SJ, Ukken FP, Rubinstein CD, Thiede G, Donohue LK, Cummings AM, and O'Connor-Giles KM (2014). Highly specific and efficient CRISPR/Cas9-catalyzed homology-directed repair in Drosophila. Genetics 196, 961–971. 10.1534/genetics.113.160713. [PubMed: 24478335]

51. Schindelin J, Arganda-Carreras I, Frise E, Kaynig V, Longair M, Pietzsch T, Preibisch S, Rueden C, Saalfeld S, Schmid B, et al. (2012). Fiji: an open-source platform for biological-image analysis. Nat Methods 9, 676–682. 10.1038/nmeth.2019. [PubMed: 22743772]

Highlights

- Endoplasmic reticulum (ER) clearance by autophagy occurs during development
- ER clearance requires PINK1 kinase
- The ubiquitin E3 ligase Parkin is required for clearance of mitochondria but not ER
- Keap1 is required for ubiquitylation of Rtnl1 and clearance of ER

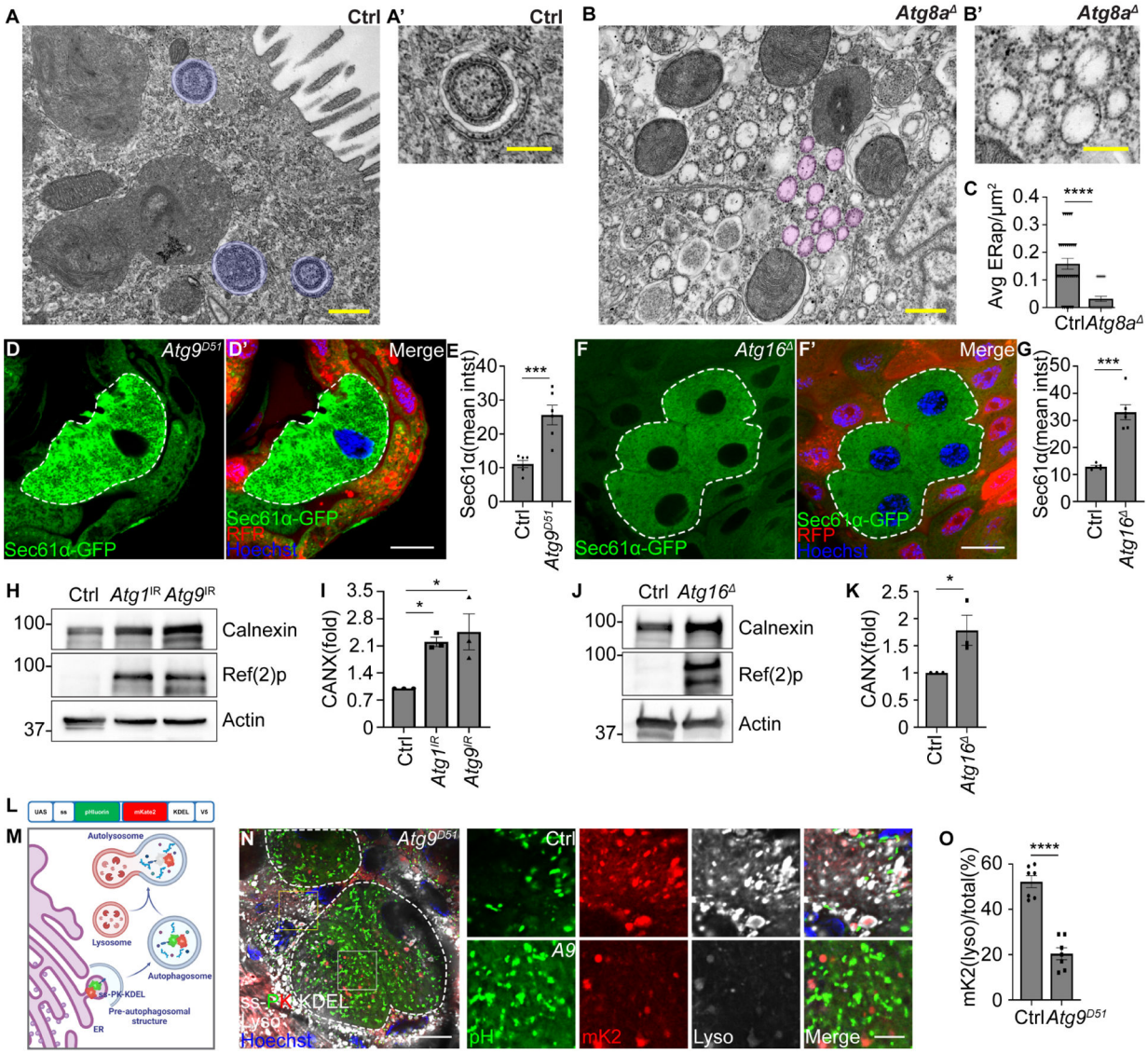

Figure 1. Autophagy regulates ER clearance during development.

(A and B) TEM images of homozygous *Atg8a*$^{\Delta}$ mutant enterocytes exhibit decreased ER in autophagic structures, and reveal increased dilated ER surrounded by ribosomes compared to control (*Atg8a*$^{\Delta}$/+) cells. Blue masks label ER-autophagosomes. Magenta masks label dilated ER.

(C) Quantification of average ER-autophagosomes per μm^2 (ERap/μm^2) in *Atg8a* mutant compared to control cells. n = 32 (Ctrl), n = 32 (*Atg8a*$^{\Delta}$) images from at least 3 animals were quantified.

(D and D') *Atg9*^{D51} mutant enterocytes (lacking RFP, white dotted line) exhibit increased Sec61α (green) compared to control cells (red).

(E) Quantification of Sec61α mean intensity (mean intst) in *Atg9* mutant cells compared to control cells. n = 6 (Ctrl) cells and n = 6 (*Atg9*^{D51}) cells were measured.

(F and F') *Atg16*$^{\Delta}$ mutant enterocytes (lacking RFP, white dotted line) possess increased Sec61α (green) compared to control cells (red).

(G) Quantification of Sec61α mean intensity (mean intst) in *Atg16* mutant cells compared to control cells. n = 5 (Ctrl), n = 6 ($Atg16^{\Delta}$) cells were measured.
(H) Calnexin and Ref(2)p levels in *Atg1* RNAi knockdown (*Atg1* IR) intestines, *Atg9* RNAi knockdown (*Atg9* IR) intestines, and control intestines analyzed by western blot.
(I) Quantification of the ratio (fold) of Calnexin (CANX)/Actin normalized to control. n = 3 independent experiments.
(J) Calnexin and Ref(2)p levels in homozygous $Atg16^{\Delta}$ mutant and control intestines analyzed by western blot.
(K) Quantification of the ratio (fold) of Calnexin (CANX)/Actin normalized to control. n = 3 independent experiments.
(L) Diagram of ER-phagy sensor.
(M) Schematic of ER-phagy detection using the ss-pHluorin-mKate2-KDEL-V5 sensor.
(N) $Atg9^{D51}$ mutant enterocytes (white dotted line) that express ss-pHluorin-mKate2-KDEL-V5 (ss-PK-KDEL) in all cells exhibit increased cell size and decreased ss-mKate2-KDEL puncta (red puncta, mK2) co-localization with lysotracker (gray) compared to control cells (smaller cells).
(O) Quantification of ss-mKate2-KDEL puncta co-localized with lysotracker in *Atg9* mutant cells compared to control cells. n = 7 (Ctrl), n = 7 ($Atg9^{D51}$), cells were measured.
All animals were staged 2 hours APF. Scale bars in (A) and (B) represent 0.5 μm and scale bars in (A') and (B') represent 0.25 μm. Scale bars in (D), (F), and (N) represent 20 μm and scale bar in inset (N) represent 5 μm. Insets in (N) are from indicated rectangles (white rectangle = *Atg9* mutant cell, yellow rectangle = control cell). Data are presented as mean ± SEM. *. $p<0.05$, ***, $p<0.001$, ****, $p<0.0001$ from One-way ANOVA corrected by Tukey's post-hoc test and unpaired, two-tailed t-test. Representative of 3 or more independent biological experiments. See also Figure S1.

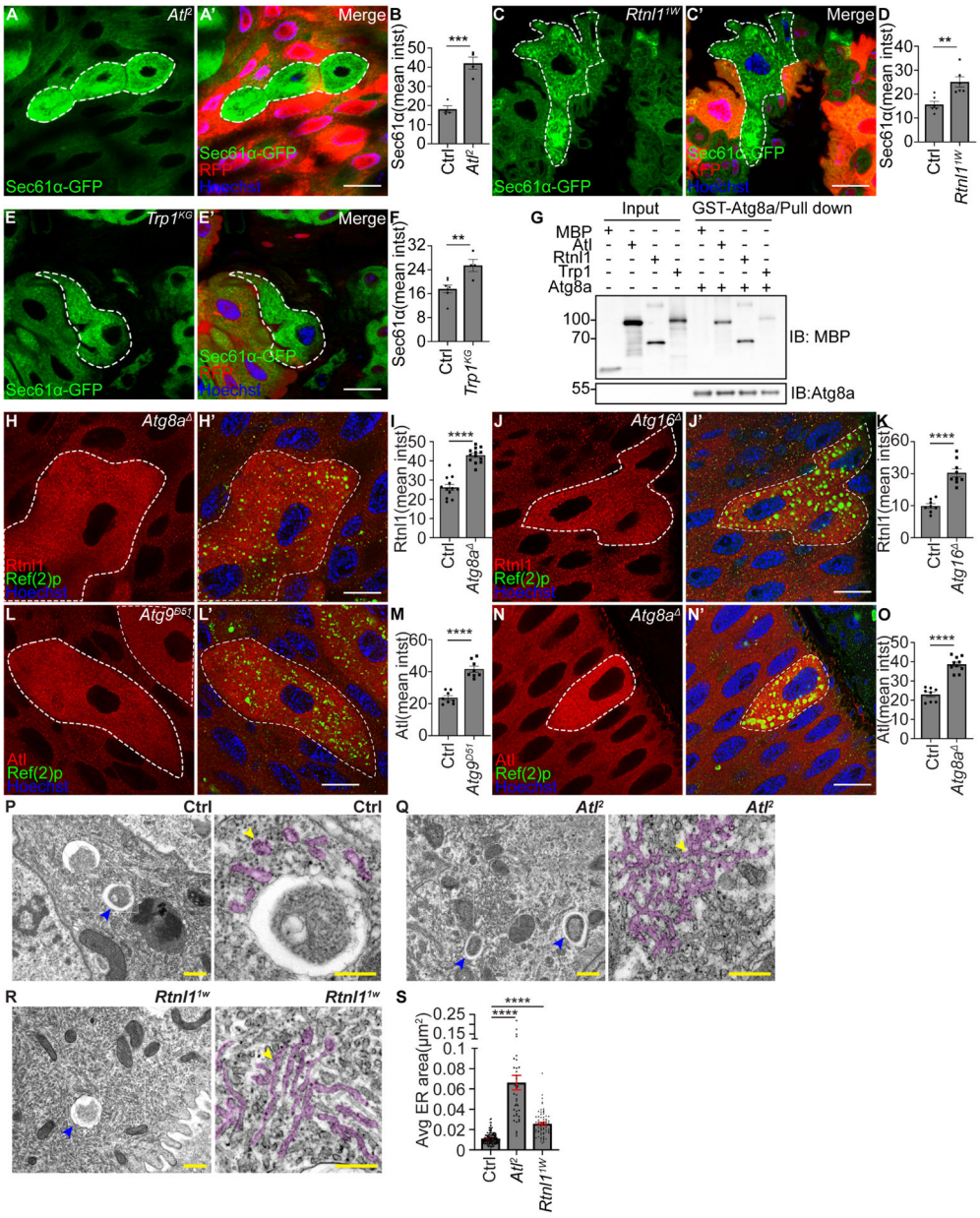

Figure 2. Atg8a binding and ER-localized proteins regulate ER clearance.

(A and A') *Atl*^{2} mutant intestine enterocytes (lacking RFP) exhibit increased Sec61α (green) compared to control cells (red).

(B) Quantification of Sec61α mean intensity (mean intst) in *Atl* mutant compared to control cells. n = 4 (Ctrl) cells and n = 4 (*Atl*^{2}) cells were measured.

(C and C') *Rtnl1*^{1w} mutant intestine enterocytes (lacking RFP) possess increased Sec61α (green) compared to control cells (red).

(D) Quantification of Sec61α mean intensity (mean intst) in *Atl* mutant compared to control cells. n = 6 (Ctrl) cells and n = 6 (*Rtnl1*^{1W}) cells were measured.

(E and E') *Trp1*^{KG} mutant enterocytes (lacking RFP) exhibit increased Sec61α-GFP (green) compared to control cells (red).

(F) Quantification of Sec61α mean intensity (mean intst) in *Trp1* mutant compared to control cells. n = 7 (Ctrl) cells and n = 4 cells (*Trp1*^{KG}) were measured.
(G) Physical interactions between MBP, MBP-Atl, MBP-Rtnl1 and MBP-Trp1 with GST-Atg8a.
(H and H') Enterocytes expressing Rtnl1–3×Flag-V5 possess increased Rtnl1 (red, detected by anti-V5 antibody) and Ref(2)p puncta (green) in *Atg8a*$^{\Delta}$ mutant compared to control cells.
Ref(2)p puncta were used to label *Atg8a*$^{\Delta}$ mutant cells.
(I) Quantification of Rtnl1 intensity in *Atg8a*$^{\Delta}$ mutant compared to control cells. n = 12 (Ctrl), n = 13 (*Atg8a*$^{\Delta}$) cells were measured.
(J and J') Enterocytes expressing Rtnl1–3×Flag-V5 possess increased Rtnl1 (red, detected by anti-V5 antibody) and Ref(2)p puncta (green) in *Atg16*$^{\Delta}$ mutant compared to control cells.
Ref(2)p puncta were used to label *Atg16*$^{\Delta}$ mutant cells.
(K) Quantification of Rtnl1 intensity in *Atg16*$^{\Delta}$ mutant compared to control cells. n = 8 (Ctrl), n = 9 (*Atg16*$^{\Delta}$) cells were quantified.
(L and L') Enterocytes expressing Atl-3×Flag-V5 possess increased Atl (red, detected by anti-V5 antibody) and Ref(2)p puncta (green) in *Atg9*^{D51} mutant compared to control cells.
Ref(2)p puncta were used to label *Atg9*^{D51} mutant cells.
(M) Quantification of Atl intensity in *Atg9*^{D51} mutant compared to control cells. n = 8 (Ctrl), n = 8 (*Atg9*^{D51}) cells were quantified.
(N and N') Enterocytes expressing Atl-3×Flag-V5 possess increased Atl (red, detected by anti-V5 antibody) and Ref(2)p puncta (green) in *Atg8a*$^{\Delta}$ mutant compared to control cells.
Ref(2)p puncta were used to label *Atg8a*$^{\Delta}$ mutant cells.
(O) Quantification of Atl intensity in *Atg8a*$^{\Delta}$ mutant compared to control cells. n = 8 (Ctrl), n = 10 (*Atg8a*$^{\Delta}$) cells were quantified
(P-R) TEM images reveal distinct ER structures in homozygous *Atl*^{2} and *Rtnl1*^{1w} mutant and control intestine cells. Blue arrowheads indicate ER in autophagic structures. Yellow arrowheads indicate ER structures. Magenta masks in the insets label rough ER structures.
(S) Quantification of 3–5 rough ER area per image in *Atl* and *Rtnl1* mutant compared to control cells. n = 132 (Ctrl), n = 39 (*Atl*^{2}), n = 67 (*Rtnl1*^{1W}) ER structures from 60 (Ctrl), 45 (*Atl*^{2}), 51 (*Rtnl1*^{1W}) images measured.
All animals were staged 2 hours APF. Mutant cells are indicated with white dotted lines. Scale bars in (A), (C), (E), (H), (J), (L) and (N) represent 20 μm. Scale bars in (P) to (R) lower magnification represent 0.5 μm, and scales bars in insets represent 0.25 μm. Data are presented as mean ± SEM. **, p<0.01, ***, p<0.001, ****, p<0.0001 from unpaired, two-tailed t-test and One-Way ANOVA corrected by Tukey's post-hoc test. Representative of 3 or more independent biological experiments. See also Figure S2.

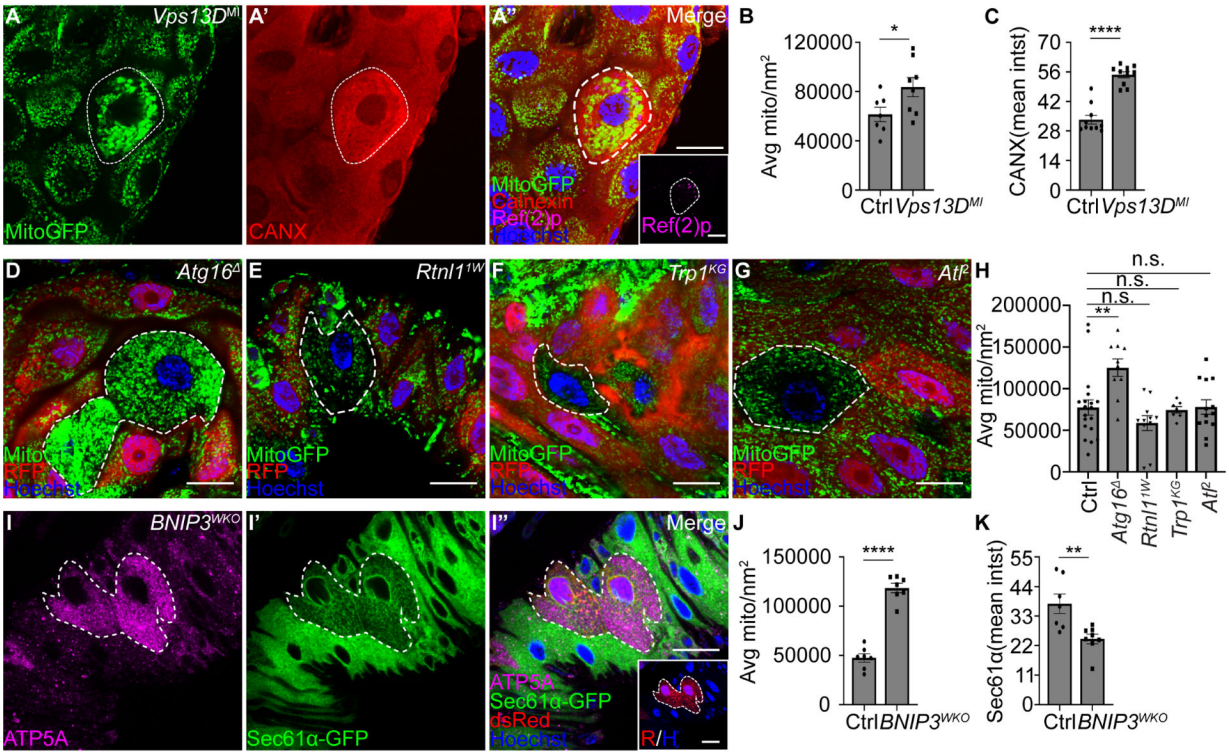

Figure 3. Selective organelle clearance requires both common regulators and distinct autophagy receptors for each organelle.

(A-A") *Vps13D*^{MI} mutant cells exhibit increased Mito-GFP (A, green), Calnexin (A', red, CANX) and Ref(2)p (magenta, inset in A") compared to control cells.

Quantification of average Mito-GFP puncta per μm^2 in *Vps13D* mutant compared to respective control cells. n = 7 (Ctrl), n = 8 (*Vps13D*^{MI}) cells were measured.

Quantification of Calnexin mean intensity (mean intst) in *Vps13D* mutant cells compared to control cells. n = 10 (Ctrl), n = 10 (*Vps13D*^{MI}) cells were measured.

(D-G) *Atg16*^{Δ}, *Rtnl1*^{1w}, *Trp1*^{KG} and *Atl*^{2} mutant enterocytes (lacking RFP) exhibit either elevated Mito-GFP (green) puncta (*Atg16*^{Δ}) or comparable Mito-GFP puncta (*Rtnl1*^{1w}, *Trp1*^{KG} and *Atl*) compared to control cells (red).

(H) Quantification of Mito-GFP puncta in *Atg16*, *Rtnl1*, *Trp1* and *Atl* mutant compared to respective control cells. n = 19 (Ctrl), n = 10 (*Atg16*^{Δ}), n = 11 (*Rtnl1*^{1w}), n = 7 (*Trp1*^{KG}), n = 13 (*Atl*^{2}) cells were measured.

(I-I") Intestine cells expressing Cas9 and dsRed (red) in *BNIP3* dual-gRNA (*BNIP3*^{WKO}) transgenic flies that express Sec61a-GFP in all cells exhibit increased levels of ATP5A puncta (I, magenta) and decreased intensity of Sec61a-GFP (I', green) compared to control cells.

(J) Quantification of average ATP5A puncta per μm^2 in *BNIP3* mutant cells compared to control cells. n = 7 (Ctrl), n = 7 (*BNIP3*^{WKO}) cells were measured.

(K) Quantification of Sec61α mean intensity (mean intst) in *BNIP3* mutant compared to control cells. n = 7 (Ctrl), n = 8 (*BNIP3*^{WKO}) cells were measured.

All animals were staged 2 hours APF. Mutant cells are indicated with white dotted lines. Scale bars in (A"), (D-G), (I) and scale bar in inset (A") and (I") represent 20 μm. Data

are presented as mean ± SEM. n.s. = not significant, *, p<0.05, **, p<0.01, ****, p<0.0001 from unpaired, twotailed t-test and One-Way ANOVA corrected by Tukey post-hoc test. Representative of 3 or more independent biological experiments. See also Figure S3.

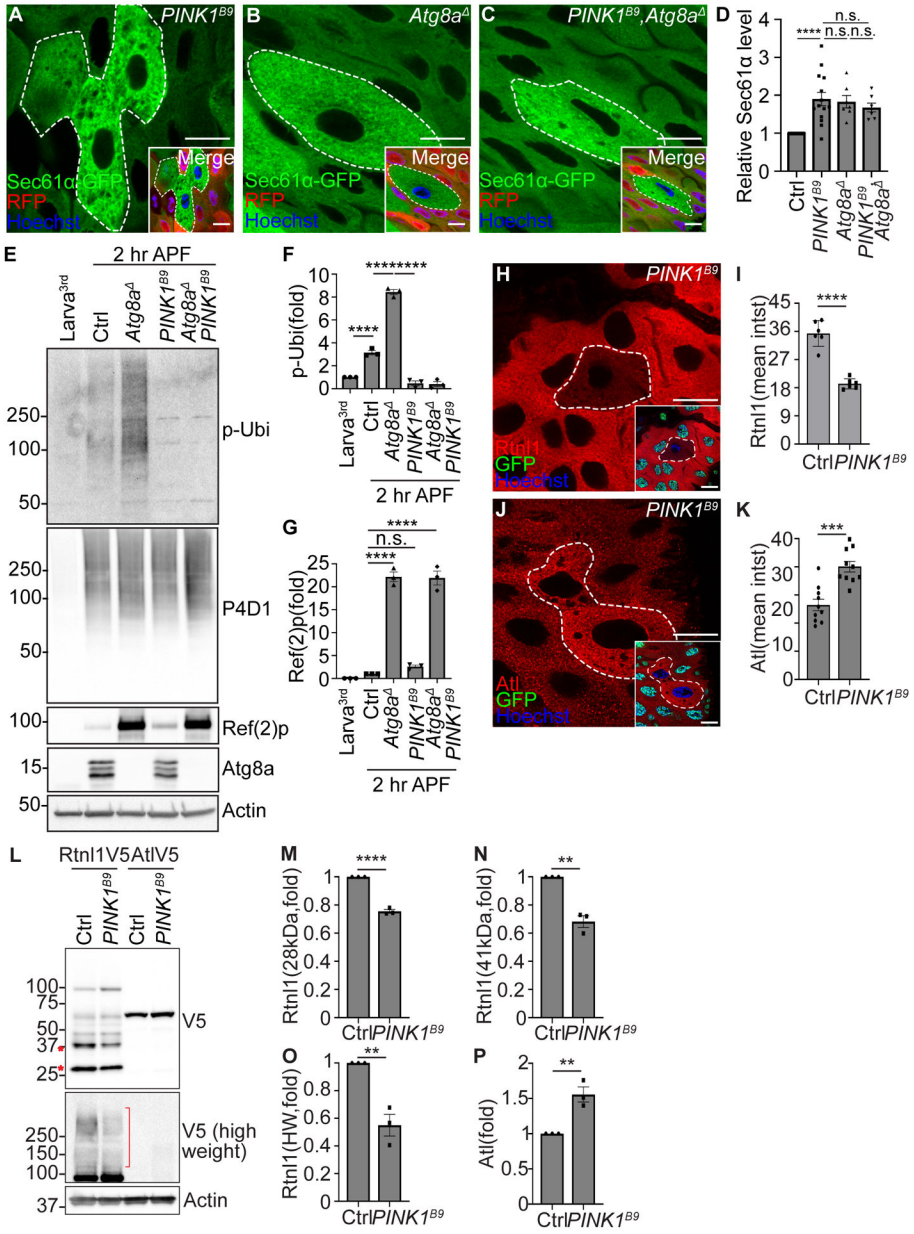

Figure 4. PINK1 regulates developmentally programmed ER clearance.

(A to C) *PINK1*^{B9} single mutant (A), *Atg8a*$^{\Delta}$ single mutant (B), and *PINK1*^{B9} and *Atg8a*$^{\Delta}$ double (C, *PINK1*^{B9}, *Atg8a*$^{\Delta}$) mutant intestine cells (lacking RFP, white dotted line) exhibit increased Sec61α (green) compared to respective control cells (red). *PINK1*^{B9} and *Atg8a*$^{\Delta}$ (C) double mutant cells possess comparable Sec61α-GFP intensity to either *PINK1*^{B9} or *Atg8a*$^{\Delta}$ single mutant icells 2 hours APF.

(D) Quantification of relative Sec61α-GFP intensity in *PINK1* single, *Atg8a* single, and *PINK1 Atg8a* double mutant cells normalized to Sec61α-GFP intensity in respective control cells. n = 14 (Ctrl), n = 14 (*PINK1*^{B9}), and n = 7 (*PINK1*^{B9}, *Atg8a*$^{\Delta}$) cells were measured.

(E) Western blot analysis of phospho-ubiquitin (serine 65, p-Ubi), pan-ubiquitin (P4D1), Ref(2)p, Atg8a and Actin in feeding third larval instar (Larva^{3rd}) *w*^{1118}, *w*^{1118} (Ctrl$^{2\ hr\ APF}$),

Atg8a$^{\Delta}$ single mutant (2 hr APF), *PINK1*^{B9} single mutant (2 hr APF), and *PINK1*^{B9} *Atg8a*$^{\Delta}$ double mutant (2 hr APF) intestines.

(F) Quantification of the ratio of phospho-ubiquitin (S65)/pan-ubiquitin (P4D1) normalized to larva. n = 3 independent experiments.

(G) Quantification of the ratio of Ref(2)p/actin normalized to larva. n = 3 independent experiments.

(H) Intestines from animals containing Rtnl1–3×Flag-V5 possess decreased Rtnl1 (red, detected by anti-V5 antibody) in *PINK1*^{B9} mutant (white dotted line, non-green nuclei) compared to control cells 2 hours APF.

(I) Quantification of Rtnl1 intensity in *PINK1*^{B9} mutant compared to control cells. n = 6 (Ctrl), n = 6 (*PINK1*^{B9}) cells were measured.

(J) Intestines from animals containing Atl-3×Flag-V5 possess increased Atl (red, detected by anti-V5 antibody) in *PINK1*^{B9} mutant (white dotted line, non-green nuclei) compared to control cells 2 hours APF.

(K) Quantification of Atl intensity in *PINK1*^{B9} mutant compared to control cells. n = 10 (Ctrl), n = 10 (*PINK1*^{B9}) cells were measured.

(L) Rtnl1 and Atl levels in male homozygous *PINK1*^{B9} mutant and control intestines 2 hours APF analyzed by western blot. Rtnl1 and Atl were detected by anti-V5 antibody.

(M) Quantification of 28 kDa Rtnl1 in *PINK1*^{B9} mutant normalized to control intestines. n = 3 independent experiments.

(N) Quantification of 41 kDa Rtnl1 in *PINK1*^{B9} mutant normalized to control intestines. n = 3 independent experiments.

(O) Quantification of high molecular weight (>100kDa, HW) Rtnl1 in *PINK1*^{B9} mutant normalized to control intestines. n = 3 independent experiments.

(P) Quantification of Atl in *PINK1*^{B9} mutant normalized to control intestines. n = 3 independent experiments.

Scales bars in (A to C, H and J) represent 20 μm. Data are presented as mean ± SEM. n.s. = not significant, **, p<0.01, ***, p<0.001, ****, p<0.0001 from One-Way ANOVA Fisher's LSD test and unpaired, two tailed t-test. Representative of 3 or more independent biological experiments. See also Figure S4.

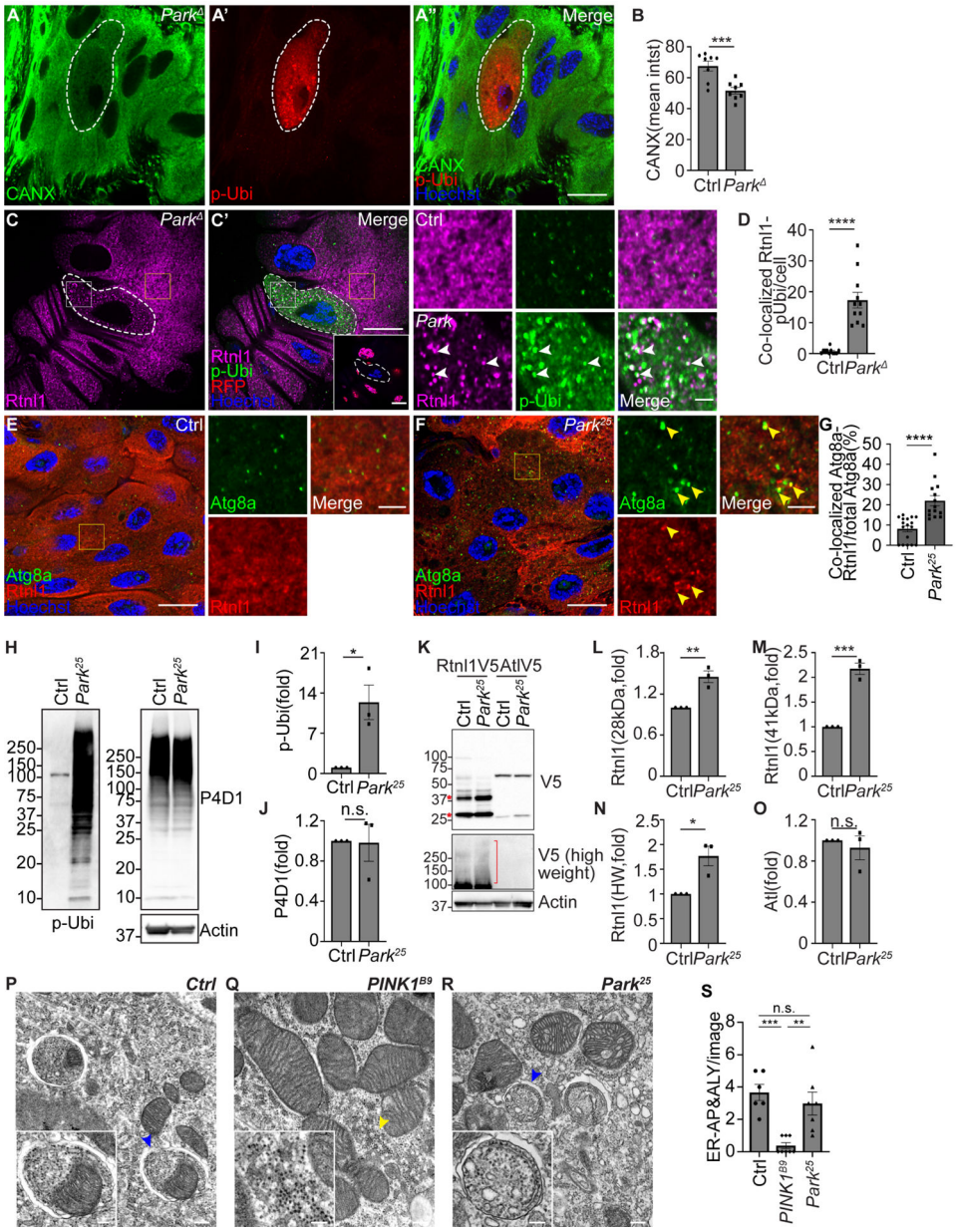

Figure 5. Parkin facilitates mitophagy and inhibits ER-phagy.

(A) *Park*$^{\Delta}$ mutant cells (white dotted line) exhibit decreased calnexin (green), increased phospho-ubiquitin (serine 65, red, p-Ubi) compared to control cells. p-Ubi was used to locate *Park*$^{\Delta}$ mutant cells.

(B) Quantification of calnexin mean intensity (mean intst) in *Park*$^{\Delta}$ mutant compared to control cells. n = 8 (Ctrl), n = 8 (*Park*$^{\Delta}$) cells were measured.

(C) Intestines from animals that contain Rtnl1–3×Flag-V5 possess decreased Rtnl1 intensity (magenta, detected by anti-V5 antibody) with increased fragmented Rtnl1 puncta that partially co-localize with phospho-ubiquitin (serine 65, green, p-Ubi) in *Park*$^{\Delta}$ mutant (white dotted line, non-red nuclei) compared to control cells.

(D) Quantification of co-localized Rtnl1 puncta with phosphorylated-ubiquitin puncta in *Park* mutant compared to control cells. n = 11 (Ctrl), n = 11 (*Park*^{4}) cells were quantified.
(E-F) *Park*^{25} mutant enterocytes (F) that contain Rtnl1–3xFlag-V5 (detected by anti-V5 antibody, red) exhibit increased Atg8a (green) puncta and increased co-localization of Atg8a with Rtnl1 puncta compared to control enterocytes (E).
(G) Quantification of the ratio of co-localized Atg8a-Rtnl1 puncta of total Atg8a puncta (%) in *Park* mutant compared to control intestine cells. n = 17 (Ctrl), n = 14 (*Park*^{25}) cells were analyzed.
(H) Western blot analysis of phospho-ubiquitin (serine 65, p-Ubi), pan-ubiquitin (P4D1), and Actin in *Park*^{25} mutant and control (Ctrl) intestines.
(I) Quantification of the ratio of phospho-ubiquitin (S65)/pan-ubiquitin (P4D1) in *Park* mutant normalized to control intestines. n = 3 independent experiments.
(J) Quantification of the ratio of pan-ubiquitin/Actin in *Park* mutant normalized to control intestines. n = 3 independent experiments.
(K) Rtnl1 and Atl levels in homozygous *Park*^{25} mutant and control intestines analyzed by western blot. Rtnl1 and Atl were detected by anti-V5 antibody.
(L) Quantification of 28 kDa Rtnl1 in *Park*^{25} mutant intestines normalized to control intestines. n = 3 independent experiments.
(M) Quantification of 41 kDa Rtnl1 in *Park*^{25} mutant intestines normalized to control intestines. n = 3 independent experiments.
(N) Quantification of high molecular weight (>100kDa, HW) Rtnl1 in *Park*^{25} mutant intestines normalized to control intestines. n = 3 independent experiments.
(O) Quantification of Atl in *Park*^{25} mutant intestines normalized to control intestines. n = 3 independent experiments.
(P-R) TEM images reveal that control *w*^{1118} intestines possess autophagosomes containing both ER and mitochondria (P), male homozygous *PINK1*^{B9} mutant intestines exhibit decreased autophagosomes/autolysosomes that contain ER (Q), and homozygous *Park*^{25} loss-of-function mutant intestines exhibit comparable autophagosomes containing ER structures (R) compared to control intestines. Blue arrowheads in (P) and (R) indicate ER in autophagic structures. Yellow arrowhead in (Q) indicates ER structures.
(S) Quantification of ER-containing autophagosomes (AP) and autolysosomes (ALY) in each image. n = 6 (Ctrl), n = 8 (*PINK1*^{B9}), n = 7 (*Park*^{25}) images were quantified.
All animals were staged 2 hours APF. Scale bars in (A”), (C), (E) and (F) represent 20 μm. Scale bars in (C), (E) and (F) insets represent 5 μm. Scale bars in (P), (Q) and (R) represent 0.2 μm, and scale bars in the inset represent 0.1 μm. Insets in (C), (E) and (F) are from indicated rectangles (white rectangle = *Park* mutant cell, yellow rectangle = control cell). Data are presented as mean ± SEM. n.s. = not significant, *, $p<0.05$, **, $p<0.01$, ***, $p<0.001$, ****, $p<0.0001$ from One-Way ANOVA corrected by Tukey post-hoc test and unpaired, two-tailed ttest. Representative of 3 or more independent biological experiments. See also Figure S5.

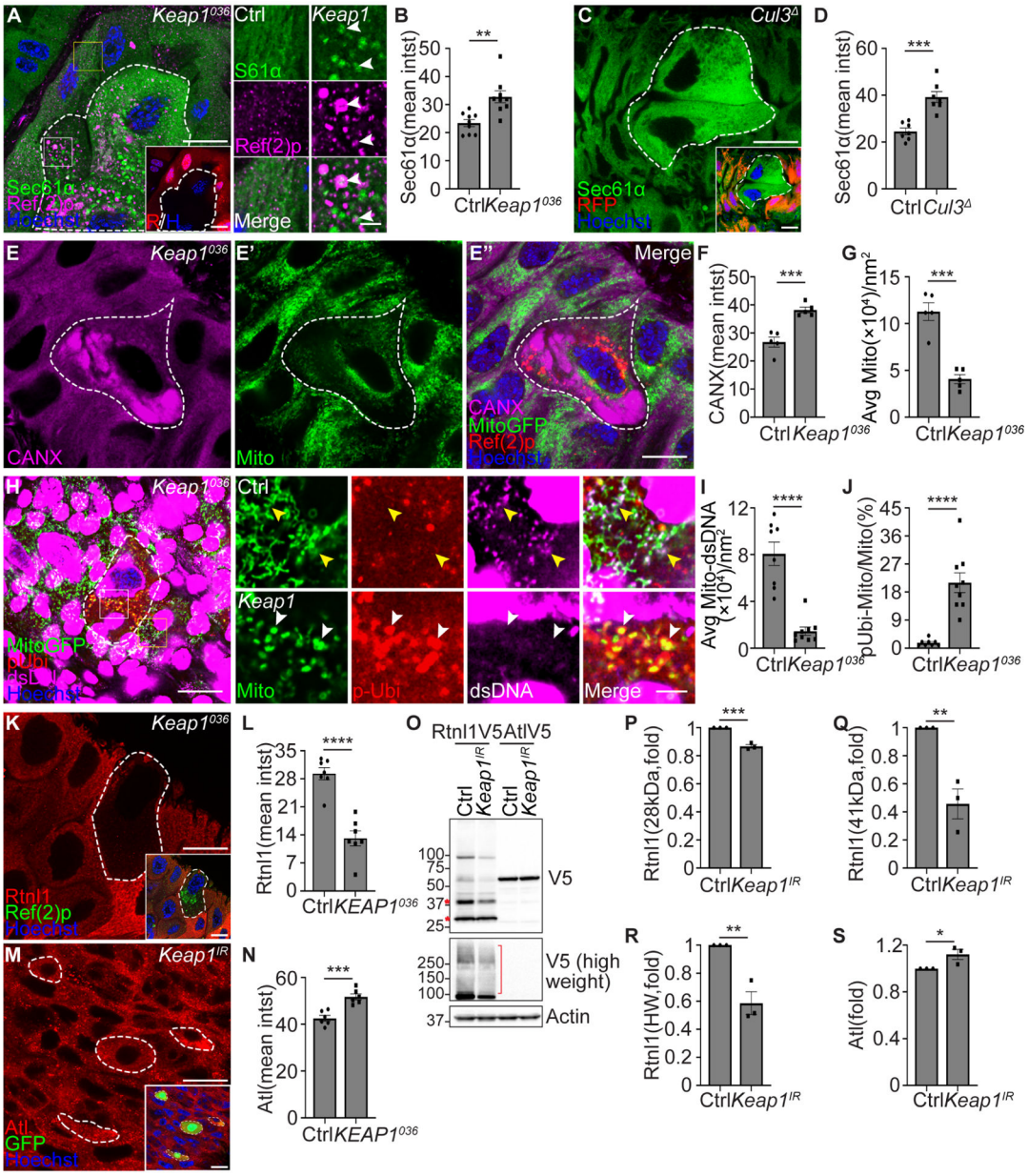

Figure 6. Keap1 facilitates ER-phagy and inhibits mitophagy.

(A) *Keap1*^{036} mutant intestine cells lacking RFP (red, white dotted line) exhibit increased Sec61α (green) and Sec61α puncta co-localization with Ref(2)p (magenta) puncta compared to the control cells. Control insets (yellow rectangle), and *Keap1* mutant insets (white rectangle).

White arrowheads indicate co-localized Sec61α and Ref(2)p puncta.

(B) Quantification of Sec61α-GFP (Sec61α) mean intensity (Sec61α intst) in *Keap1*^{036} mutant compared to control cells. n = 9 (Ctrl), n = 9 (*Keap1*^{036}) cells were measured.

(C) Animals that express Sec61α-GFP in all cells exhibit increased Sec61α-GFP (green) in *Cul3*$^{\Delta}$ mutant enterocytes (white dotted line, non-red) compared to control cells.

(D) Quantification of Sec61α-GFP intensity in *Cul3*$^{\Delta}$ mutant compared to control cells. n = 7 (Ctrl), n = 7 (*Cul3*$^{\Delta}$) cells were quantified.
(E-E") *Keap1*^{036} mutant intestine cells exhibit increased calnexin (magenta, CANX) and increased Ref(2)p puncta (red), and decreased Mito-GFP (green, Mito) puncta. Ref(2)p was used to label the *Keap1* mutant cells.
(F) Quantification of calnexin (CANX) mean intensity (CANX intst) in *Keap1* mutant compared to control cells. n = 5 (Ctrl), n = 5 (*Keap1*^{036}) cells were measured.
(G) Quantification of average Mito-GFP puncta (Mito) per nm^2 (Avg Mito/nm^2) in *Keap1* mutant compared to control cells. n = 5 (Ctrl), n = 5 (*Keap1*^{036}) cells were measured.
(H) *Keap1*^{036} mutant intestine cells possess decreased mitochondrial DNA (dsDNA, magenta) co-localization with Mito-GFP puncta (green), and increased phospho-ubiquitin (serine 65, red, p-Ubi) co-localization with Mito-GFP puncta compared to control cells. Yellow arrowheads indicate co-localized dsDNA puncta and Mito-GFP puncta. White arrowheads indicate co-localized phospho-ubiquitin puncta and Mito-GFP puncta with lack of dsDNA.
(I) Quantification of average Mito-GFP co-localization with dsDNA puncta per nm^2 (Avg Mito-dsDNA/nm^2) in *Keap1* mutant compared to control cells. n = 6 (Ctrl), n = 7 (*Keap1*^{036}) cells were measured.
(J) Quantification co-localized phospho-ubiquitin puncta and Mito-GFP puncta ratio of total Mito-GFP puncta (pUbi-Mito/Mito%) in *Keap1* mutant compared to control cells. n = 8 (Ctrl), n = 9 (*Keap1*) cells were measured.
(K) Intestines from animals containing Rtnl1–3×Flag-V5 possess decreased Rtnl1 (red, detected by anti-V5 antibody) in *Keap1*^{036} mutant (white dotted line) compared to control cells. Ref(2)p was used to label mutant cells.
(L) Quantification of Rtnl1 intensity in *Keap1* mutant compared to control cells. n = 7 (Ctrl), n = 7(*Keap1*^{036}) cells were measured.
(M) Intestines from animals containing Atl-3×Flag-V5 possess increased Atl (red, detected by anti-V5 antibody) in *Keap1* RNAi knockdown enterocytes (white dotted line, non-green nuclei) compared to control cells.
(N) Quantification of Atl intensity in *Keap1* RNAi cells compared to control cells. n = 6 (Ctrl), n = 6 (*Keap1*^{036}) cells were measured
(O) Rtnl1 and Atl levels in *Keap1* RNAi knockdown and control intestines analyzed by western blot. Rtnl1 and Atl were detected by anti-V5 antibody.
(P) Quantification of 28 kDa Rtnl1 in *Keap1* RNAi intestines normalized to control intestines. n = 3 (Ctrl), n = 3 (*Keap1*^{036}) independent experiments.
(Q) Quantification of 41 kDa Rtnl1 in *Keap1* RNAi intestines normalized to control intestines. n = 3 (Ctrl), n = 3 (*Keap1*^{036}) independent experiments.
(R) Quantification of high molecular weight (>100kDa, HW) Rtnl1 in *Keap1* RNAi intestines normalized to control intestines. n = 3 (Ctrl), n = 3 (*Keap1*^{IR}) independent experiments.
(S) Quantification of Atl in *Keap1* RNAi intestines normalized to control intestines. n = 3 (Ctrl), n = 3 (*Keap1*^{IR}) independent experiments.
All animals were staged 2 hours APF. Scale bars in (A and inset at the right corner), (C and inset), (E"), (H), (K and inset), (M and inset) represent 20 μm. Scale bars in (A, right panel), (H, right panel) insets represent 5 μm. Insets in (A) and (H) are from indicated

rectangles (white rectangle = *Keap1* mutant cell, yellow rectangle = control cell). Data are presented as mean ± SEM. n.s. = not significant, **, p<0.01, ***, p<0.001, ****, p<0.0001, from One-Way ANOVA corrected by Tukey post-hoc test and unpaired, two-tailed t-test. Representative of 3 or more independent biological experiments. See also Figure S6.

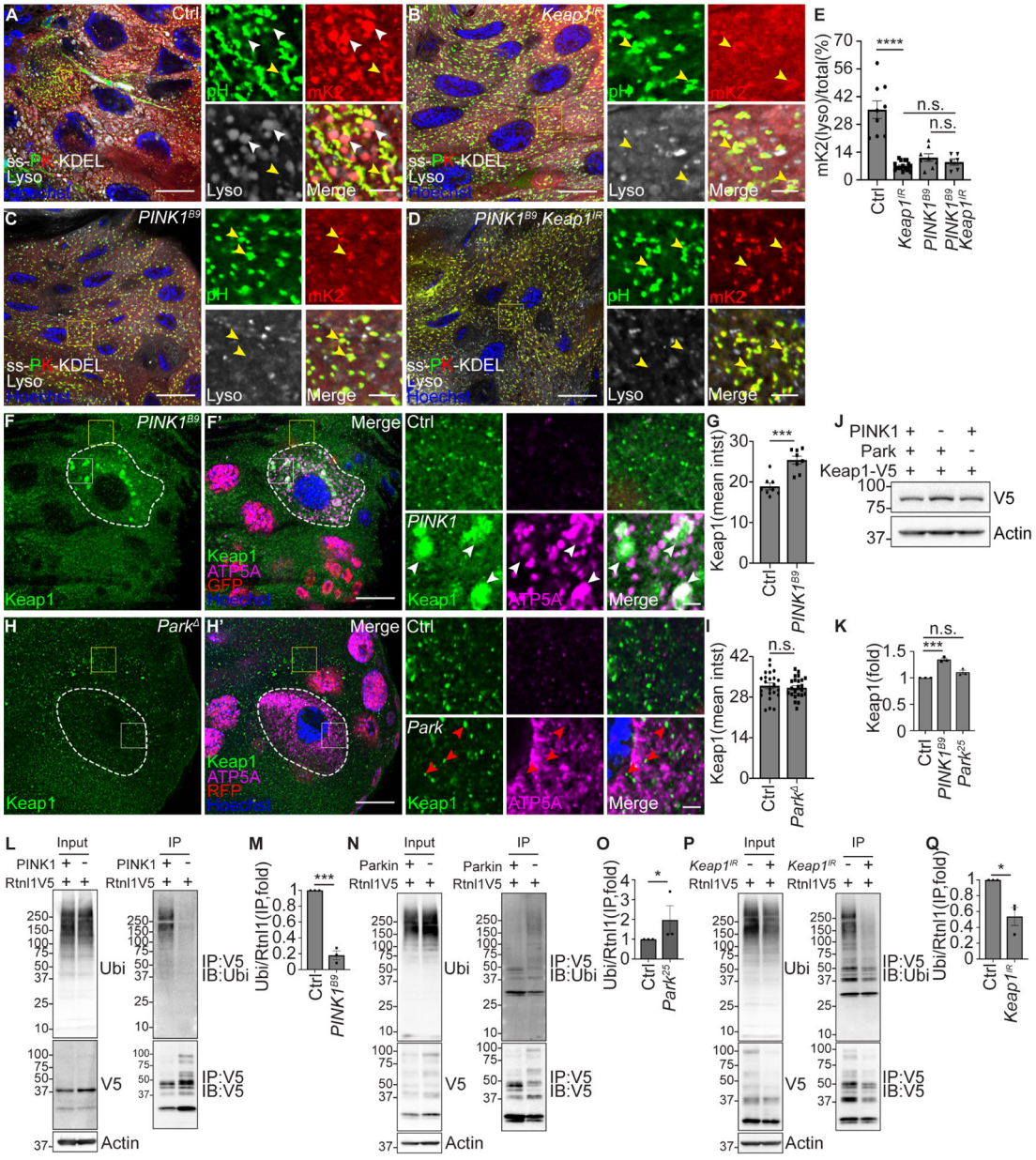

Figure 7. PINK1 influences Keap1 localization, Rtnl1 ubiquitylation and ER clearance.

(A-D) Male *Keap1* knockdown (*Keap1*^{IR}, B) intestines expressing *Keap1* RNAi, male *PINK1*^{B9} loss-of-function intestines (C) and male *PINK1*^{B9} mutant intestines expressing *Keap1* RNAi (*PINK1*^{B9}*, Keap1*^{IR}, D) that express ss-pHluorin-mKate2-KDEL-V5 exhibit decreased red puncta co-localization with lysotracker (gray) compared to control *Luciferase RNAi* intestine cells (A). *PINK1* and *Keap1* double mutant intestines exhibit similar decrease in ER-phagy flux measured by the ER-phagy sensor compared to either of the *PINK1* or *Keap1* single mutant intestines. Insets are from yellow rectangles. White arrowheads indicate co-localized red puncta and lysotracker puncta. Yellow arrowheads indicate co-localized green and red puncta.

(E) Quantification of ratio of lysotracker co-localized red with ss-mKate2-KDEL puncta/total ssmKate2-KDEL puncta (mK2(lyso)/total%). n = 9 (Ctrl), n = 17 (*Keap1*^{IR}), n = 8 (*PINK1*^{B9}), n = 6 (*PINK1*^{B9}, *Keap1*^{IR}) cells were measured.

(F and F') Intestines from animals that contain Keap1–3×Flag-V5 possess increased and large Keap1 puncta (green, detected by anti-V5 antibody) that co-localize with increased ATP5A puncta (magenta) in *PINK1*^{B9} mutant (white dotted line) compared to control cells.

(G) Quantification of Keap1 intensity in *PINK1* mutant compared to neighboring control cells. n = 8 (Ctrl), n = 8 (*PINK1*^{B9}) cells were measured.

(H and H') Intestines from animals that contain Keap1–3×Flag-V5 exhibit similar Keap1 intensity (green, detected by anti-V5 antibody) and some co-localization with ATP5A puncta (magenta) in *Park*$^{\Delta}$ mutant enterocytes (white dotted line, non-red in nuclei) compared to control cells.

(I) Quantification of Keap1 intensity in *Parkin* mutant compared to control cells. n = 23 (Ctrl), n = 23 (*Park*$^{\Delta}$) cells were analyzed.

(J) Keap1 levels in male homozygous *PINK1*^{B9}, *Park*^{25} mutant and control intestines analyzed by western blot. Keap1 was detected by anti-V5 antibody.

(K) Quantification of Keap1 in *PINK1* and *Parkin* mutant intestines normalized to control intestines. n = 3 independent experiments.

(L) Rtnl1 was immunoprecipitated from either control or *PINK1*^{B9} mutant intestines. Whole lysates (Input) and immunoprecipitated proteins (IP) were immunoblotted with anti-ubiquitin (P4D1), anti-V5, and anti-Actin antibodies.

(M) Quantification the ratio of ubiquitin (IP)/total Rtnl1-V5 (IP) in *PINK1*^{B9} mutant intestines normalized to control intestines. n = 3 independent experiments.

(N) Rtnl1 was immunoprecipitated from either control or *Park*^{25} mutant intestines. Whole lysates (Input) and immunoprecipitated proteins (IP) were immunoblotted with anti-ubiquitin (P4D1), anti-V5, and anti-Actin antibodies.

(O) Quantification of the ratio of ubiquitin (IP)/total Rtnl1-V5 (IP) in *Park*^{25} mutant normalized to control intestines. n = 3 (Ctrl), n = 3 (*Park*^{25}) independent experiments.

(P) Rtnl1 was immunoprecipitated from either control or *Keap1* RNAi intestines. Whole lysates (Input) and immunoprecipitated proteins (IP) were immunoblotted with anti-ubiquitin (P4D1), anti-V5, and anti-Actin antibodies.

(Q) Quantification of the ratio of ubiquitin (IP)/total Rtnl1-V5 (IP) in *Keap1* knockdown intestines normalized to control intestines. n = 3 (Ctrl), n = 3 (*Keap1*^{IR}) independent experiments.

All animals were staged 2 hours APF. Scale bars in (A-D), (F') and (H') represent 20 μm. Scale bars in (A-D), (F) and (H) insets represent 5 μm. Insets are from indicated rectangles (white rectangle in (F) and (H) = mutant cell, yellow rectangle in (F) and (H) = control cell). Data are presented as mean ± SEM. n.s. = not significant, **, $p<0.01$, ***, $p<0.001$, ****, $p<0.0001$, from One-Way ANOVA corrected by Tukey post-hoc test, Kruskal-Wallis H test and unpaired, two-tailed t-test. Representative of 3 or more independent biological experiments. See also Figure S7.

KEY RESOURCES TABLE

REAGENTS or RESOURCE	SOURCE	IDENTIFIER
Antibodies		
Ref(2)p/p62	Abcam	ab178440
Atg8a	Cell Signaling	13733
ATP5a	Abcam	Ab14748
Calnexin	Developmental Studies Hybridoma Bank	Cnx99A 6-2-1
GFP	Abcam	ab150169
GFP	Roche	11814460001
V5	Invitrogen	R960–25
V5	Cell signaling	13202
FLAG	Cell signaling	14793
Calnexin	Developmental Studies Hybridoma Bank	Cnx99A 6-2-1
Phospho-ubiquitin (serine 65, E2J6T)	Cell Signaling	62802
Phospho-ubiquitin (serine 65, E5T1W)	Cell Signaling	70973
Ubiquitin (P4D1)	Cell Signaling	3936
Conjugated ubiquitin (UBCJ2)	Enzo Life Science	ENZ-ABS840–0100
autoimmune double stranded DNA	Developmental Studies Hybridoma Bank	autoanti-dsDNA
Actin	Developmental Studies Hybridoma Bank	JLA20
Anti-mouse Alexa Fluor 488	Invitrogen	A-11029
Anti-rabbit Alexa Fluor 488	Invitrogen	A-27034
Anti-rabbit Alexa Fluor 546	Invitrogen	A-11035
Anti-mouse Alexa Fluor 546	Invitrogen	A-11030
Anti-mouse Alexa Fluor 647	Invitrogen	A-S28181
Anti-rabbit Alexa Fluor 647	Invitrogen	A-27040
Anti-chicken Alexa Fluor 488	Abcam	ab150169
Goat anti-Rabbit IgG (H+L) Secondary Antibody, HRP	Invitrogen	31460
Goat anti-Mouse IgG (H+L) Secondary Antibody, HRP	Invitrogen	31430
MBP Monoclonal Antibody (HRP conjugated)	NEB	E8038
MBP magnetic beads	NEB	E8037S
Glutathione Magnetic Agarose Beads	Thermo Scientific	78602
ChromoTek V5-Trap Agarose	Proteintech	V5ta-20
Bacterial and virus strains		
BL21 Competent *E. coli*	NEB	C2530H
Chemicals, peptides and recombinant proteins		
Glutathione (reduced)	Thermo Scientific	78259
D-(+)-Maltose monohydrate	SUPELCO	47288
Normal goat serum	Life technologies	PCN5000
PBS	GIBCO	70011

REAGENTS or RESOURCE	SOURCE	IDENTIFIER
Hoechst	Invitrogen	33342
Vectashield	Vector Laboratories	H-1200
LysoTracker Deep Red	Invitrogen	L12492
Halt™ Protease and Phosphatase Inhibitor Single-Use Cocktail, EDTA-Free (100X)	Thermo Scientific	78445
PMSF	Roche	10837091001
Experimental Models: Organisms/Strains		
PINK1-GFP	Hong Xu	N/A
Rtnl1–3×Flag-V5	This study	N/A
Atl-3×Flag-V5	This study	N/A
Keap1–3×Flag-V5	This study	N/A
UAS-Bip-pHluorin-mKate2-KDEL-V5	This study	N/A
Atg9^{D51}	Guangchao Chen	N/A
Vps34^{m22}	Thomas Neufeld	N/A
Atl^{2}	James McNew	N/A
Rtnl1^{1W}	James McNew	N/A
Park^{25}	Leo Pallanck	N/A
PINK1^{B9}	Jongkyeong Chung	N/A
PINK1^{5}	Ming Guo	N/A
Atg16$^{\Delta}$	Eric Baehrecke	N/A
Atg8$^{\Delta}$	This study	N/A
Park$^{\Delta}$	This study	N/A
BNIP3$^{\Delta}$	This study	N/A
Keap1^{036}	Dirk Bohmann	N/A
ARE-GFP	Dirk Bohmann	N/A
Cnc^{1223}	Fengwei Yu	N/A
Cul3^{GFT2}, FRT40A	Bloomington *Drosophila* Stock Center	23866
vasa-Cas9	Bloomington *Drosophila* Stock Center	56552
vasa-Cas9	Bloomington *Drosophila* Stock Center	51324
UAS-Cas9	Bloomington *Drosophila* Stock Center	67078
UAS-mitoGFP	Bloomington *Drosophila* Stock Center	8442
UAS-mitoGFP	Bloomington *Drosophila* Stock Center	8443
Vps13D^{MI11101}	Bloomington *Drosophila* stock center	56282
Df(3L)BSC631	Bloomington *Drosophila* stock center	25722
Park (TKO.GS00852)	Bloomington *Drosophila* stock center	77064
Atg1 RNAi	Vienna *Drosophila* Resource Center	16133
Atg9 RNAi	Vienna *Drosophila* Resource Center	10045
PINK1 RNAi	Bloomington *Drosophila* stock center	38262
PINK1 RNAi	Bloomington *Drosophila* stock center	55886

REAGENTS or RESOURCE	SOURCE	IDENTIFIER
Vps13D RNAi	Vienna *Drosophila* RNAi Cente	41792
Luciferase RNAi	Bloomington *Drosophila* stock center	31603
BNIP3 (WKO.3-C11)	Bloomington *Drosophila* stock center	82537
Keap1 RNAi	Bloomington *Drosophila* stock center	40932
His2Av-mRFP, FRT2A	Bloomington *Drosophila* stock center	34498
HsFlp, Ubi-nlsRFP, FRT19A	Bloomington *Drosophila* stock center	31416
HsFlp, His2Av-GFP, FRT19A	Bloomington *Drosophila* stock center	32045
hsFlp(D5)	Bloomington *Drosophila* stock center	55814
hsFlp; FRT42D,Ubi-nlsRFP	Eric Baehrecke	N/A
hsFlp; Ubi-nlsRFP, FRT40A	Eric Baehrecke	N/A
hsFlp;;FRT82B, Ubi-nlsRFP	Eric Baehrecke	N/A
hsFlp;;His2Av-mRFP, FRT2A	This study	N/A
hsFlp;;Sec61a-GFP, Act(CD2)Gal4, UAS-dsRed	This study	N/A
hsFlp; UAS-Cas9; Sec61a-GFP, Act(CD2)Gal4, UAS-dsRed	This study	N/A
hsFlp; FRT42D	This study	N/A
hsFlp;;FRT82B	This study	N/A
hsFlp;;FRT2A	This study	N/A
FRT19A;hsFlp	This study	N/A
Tub-Gal4	Eric Baehrecke	N/A
NP1-Gal4	Eric Baehrecke	N/A
Sec61α-GFP	Vienna *Drosophila* RNAi Cente (VDRC)	318343
$Trp1^{K13305}$, FRT40A	Kyoto *Drosophila* Genetic Resource Center	114350
Recombinant DNA		
U6droBsagRNA	Drosophila Genomics Resources Center	1341
pCFD3.1-w-dU6:3gRNA	Addgene	123366
pUASTattB	Drosophila Genomics Resources Center	1419
pCR™ 2.1-TOPO™ TA vector	Invitrogen	450641
Oligonucleotides (See Table S2 for a list of oligonucleotides)		
Software and Algorithms		
Image J	NIH	https://imagej.nih.govij/
Image Studio Lite Ver 5.2	LI-COR	https://www.licor.com/bio/image-studio-lite/
Prism	Graphpad Software	https://www.graphpac.com/scientific-software/prism/
ZEN	Zeiss	https://www.zeiss.com/microscopy/us/prodats/microscopesoftware/;en.html

REAGENTS or RESOURCE	SOURCE	IDENTIFIER
NIS-Elements	Nikon	https://www.microscope.healthcare.nikon.com/products/software/nis-elements